Human Molecular Genetics, 2016, Vol. 25, No. 23 5094–5110

doi: 10.1093/hmg/ddw273
Advance Access Publication Date: 13 August 2016
Original Article

ORIGINAL ARTICLE

Haploinsufficiency of Klippel-Trenaunay syndrome gene *Aggf1* inhibits developmental and pathological angiogenesis by inactivating PI3K and AKT and disrupts vascular integrity by activating VE-cadherin

Teng Zhang[1,2,†], Yufeng Yao[3,†], Jingjing Wang[3,†], Yong Li[2,†], Ping He[1,2], Vinay Pasupuleti[1,2], Zhengkun Hu[3], Xinzhen Jia[3], Qixue Song[3], Xiao-Li Tian[1,2], Changqing Hu[3], Qiuyun Chen[1,2,*] and Qing Kenneth Wang[1,2,3,4,*]

[1]The Center for Cardiovascular Genetics, Department of Molecular Cardiology, NE40, Lerner Research Institute, Cleveland Clinic, Cleveland, OH, USA, [2]Department of Molecular Medicine, Cleveland Clinic Lerner College of Medicine, OH, USA, [3]Key Laboratory of Molecular Biophysics of the Ministry of Education, College of Life Science and Technology and Center for Human Genome Research, Huazhong University of Science and Technology, Wuhan, Hubei Province, P. R. China and [4]Department of Genetics and Genome Sciences, Case Western Reserve University School of Medicine, Cleveland, OH, USA

*To whom correspondence should be addressed at: Qiuyun Chen, The Center for Cardiovascular Genetics, Department of Molecular Cardiology, NE40, Lerner Research Institute, Cleveland Clinic; Cleveland, OH 44195, USA. Tel: -1 2164442122; Fax -1 2166361231; Email: chenq3@ccf.org; Qing Kenneth Wang, Center for Human Genome Research, Huazhong University of Science and Technology, Wuhan, 430074, Hubei Province, P. R. China. Tel: +86 2787793502; Fax: +86 2787793502; Email: wangq2@ccf.org, qkwang@hutst.edu.cn

Abstract

Aggf1 is the first gene identified for Klippel-Trenaunay syndrome (KTS), and encodes an angiogenic factor. However, the *in vivo* roles of *Aggf1* are incompletely defined. Here we demonstrate that *Aggf1* is essential for both physiological angiogenesis and pathological tumour angiogenesis *in vivo*. Two lines of *Aggf1* knockout (KO) mice showed a particularly severe phenotype as no homozygous embryos were observed and heterozygous mice also showed embryonic lethality (haploinsufficient lethality) observed only for *Vegfa* and *Dll4*. *Aggf1*$^{+/-}$ KO caused defective angiogenesis in yolk sacs and embryos. Survived adult heterozygous mice exhibit frequent haemorrhages and increased vascular permeability due to increased phosphorylation and reduced membrane localization of VE-cadherin. AGGF1 inhibits VE-cadherin phosphorylation, increases plasma membrane VE-cadherin in ECs and in mice, blocks vascular permeability induced by ischaemia-reperfusion (IR), restores depressed cardiac function and contraction, reduces infarct sizes, cardiac fibrosis and necrosis, haemorrhages, edema, and macrophage density associated with IR. Mechanistically, AGGF1 promotes angiogenesis by activating catalytic p110α subunit and p85α regulatory subunit of PI3K, leading to activation of AKT, GSK3β and p70S6K. AKT activation is significantly reduced in heterozygous KO mice and isolated KO ECs, which can be rescued by exogenous AGGF1. ECs from KO mice show reduced capillary angiogenesis, which is rescued by AGGF1 and AKT. Tumour growth/angiogenesis is reduced in heterozygous mice, which was associated with reduced activation of p110α, p85α and AKT. Together with recent identification of somatic

[†]The authors wish it to be known that, in their opinion, the first four authors should be regarded as joint First Authors.
Received: May 30, 2016. **Revised:** July 24, 2016. **Accepted:** August 5, 2016

mutations in p110α (encoded by *PIK3CA*), our data establish a potential mechanistic link between *AGGF1* and *PIK3CA*, the two genes identified for KTS.

Introduction

Development of the vascular system is one of the earliest events in embryogenesis and organogenesis, and requires vasculogenesis and angiogenesis. Abnormal development of the vascular system results in various human vascular diseases. KTS (Klippel-Trenaunay syndrome, MIM *149000) is a congenital vascular disease that affects primarily the capillary vessels and veins (1–5). KTS is considered as one of the most severe vascular diseases and causes significant morbidity and mortality, mostly in children (3). The aetiology of KTS is poorly understood, but our studies have found that genomic variants in the *AGGF1* gene are associated with significant risk of KTS, defining *AGGF1* as the first susceptibility gene for KTS (6). We showed that the chromosomal mutation that causes KTS acted by a gain of function mechanism by increasing AGGF1 expression (6,7).

The *AGGF1* gene was originally named as *VG5Q* (referring to as a vascular gene on chromosome 5q) associated with KTS, and encodes an angiogenic factor (AnGiogenic Factor with G Patch and FHA Domains 1) with 714 amino acids (1,6,8). Purified AGGF1 protein can promote angiogenesis in the chick chorioallantoic membrane (CAM) and matrigel-based capillary tube formation assays *in vitro* as strongly as VEGFA (6). The pathogenesis of KTS is associated with increased angiogenesis (hyper-vascularization) and increased AGGF1 expression (6). *AGGF1* expression is regulated by transcriptional factor GATA1 (9). *AGGF1* mRNA is highly expressed in endothelial cells (ECs) (6). Knockdown of *GATA1* expression in endothelial cells (ECs) by siRNA resulted in decreased *AGGF1* expression, which led to EC apoptosis as well as inhibition of EC migration and endothelial capillary vessel formation, which were all rescued by recombinant AGGF1 in media (9). We showed that ECs with overexpression of *AGGF1* had significantly more capillary tube formation in a matrigel angiogenesis assay (1) and *AGGF1* gene delivery via direct intramuscular injection of *AGGF1* expression plasmid DNA increased angiogenesis in a hindlimb ischaemia model for peripheral artery disease (10). We further showed that morpholino knockdown of *Aggf1* expression in zebrafish embryos affected vascular development and differentiation of multipotent hemangioblasts form the mesoderm (7,11). The *in vivo* function of *AGGF1* has, however, remained to be further defined as no knockout (KO) mice targeting *Aggf1* have been reported yet and it is unknown whether *AGGF1* is an essential gene for angiogenesis and/or other biological functions. Note that to follow the standards in the field, AGGF1 is referred to as either the human or mouse protein, italicized *AGGF1* is referred to as the human gene, and italicized *Aggf1* is referred to as the mouse gene.

To characterize the function of *Aggf1 in vivo*, we have created and characterized two independent lines of KO mice. *Aggf1* deficient embryos exhibited defective angiogenesis during development and manifested vascular abnormalities in adulthood as well. In addition, our evidence indicates that *Aggf1* is involved in pathological angiogenesis (tumour growth). We further established that AGGF1 regulates angiogenesis and vascular development by activating the PI3K and AKT signalling pathway and maintains vascular integrity and homeostasis by regulating VE-cadherin *in vitro* and *in vivo*. We also showed that AGGF1 protein therapy can restore cardiac function and contraction in an ischaemia-reperfusion model by increasing angiogenesis and by blocking vascular permeability.

Results

Aggf1 gene KO results in early haploinsufficient embryonic lethality

To elucidate the physiologic role of *Aggf1 in vivo*, we developed KO mice targeting *Aggf1*. An insertion mutation was introduced into intron 11 of the *Aggf1* gene on mouse chromosome 13 in mouse embryonic stem (ES) cells by gene-trapping using a vector that contains a splicing adaptor followed by a *β-geo* reporter gene (referred to as $Aggf1^{Geo/+}$) (Fig. 1). The mutation results in a truncated AGGF1 protein with the G-patch domain and C-terminus replaced with β-Geo (Fig. 1) that produced a fusion protein with 569 N-terminal amino acids of AGGF1 fused to 1,327 amino acids of the β-galactosidase-neomycin (β-geo) protein (an estimated molecular weight of 212 kDa). Western blotting using an antibody against the C-terminus of AGGF1 revealed about 2-fold reduction of AGGF1 protein expression in $Aggf1^{Geo/+}$ embryos (embryonic day 12.5 or E12.5) (Fig. 1C). Similar analysis using an antibody against the N-terminus of AGGF1 revealed expression of the AGGF1-β-Geo fusion protein and wild type AGGF1 protein in $Aggf1^{Geo/+}$ mice (Fig. 1D). Western blotting using an antibody against β-galactosidase detected the AGGF1-β-geo fusion protein only in $Aggf1^{Geo/+}$ mice (Fig. 1E).

One male gene-trapping founder (a nearly complete transmitter of ES-derived sperm based on skin colour) was bred to a normal female C57BL/6 mouse, which generated nine embryos: five normal-looking embryos, one very small embryo, and three dead embryos (Fig. 1F). Two dead embryos were resorbed. Some residual tissue was obtained from the other dead embryo. Tissue samples were also obtained from the six other embryos for genotyping. The dead embryo with some residual tissue and the small embryo were both $Aggf1^{Geo/+}$, and the five normal-looking embryos were all wild-type $Aggf1^{+/+}$ (Fig. 1F). These data directly demonstrate embryonic lethality of some heterozygous $Aggf1^{Geo/+}$ embryos (haploinsufficient lethality).

To further show haploinsufficient/heterozygous lethality, we generated 35 litters with 220 mice from $Aggf1^{Geo/+}$ x $Aggf1^{Geo/+}$ crosses. No homozygous $Aggf1^{Geo/Geo}$ mice were born (Table 1A), indicating that *Aggf1* is essential for mouse embryonic development. Interestingly, the ratio of heterozygous $Aggf1^{Geo/+}$ mice was lower than expected (1.34 shown versus 2.00 expected, Table 1A). These data indicate that 1/3 of heterozygous $Aggf1^{Geo/+}$ embryos died before birth, again demonstrating haploinsufficient lethality.

To determine at which stage the homozygous $Aggf1^{Geo/Geo}$ embryos died, we performed sibling mating within F1 heterozygous $Aggf1^{Geo/+}$ mice. Embryos at developmental stages of E8.5, E9.5, E10.5, E11.75, E12.75, and E14.5 were isolated and genotyped. No homozygous $Aggf1^{Geo/Geo}$ embryos were identified. These results support that homozygous $Aggf1^{Geo/Geo}$ mice die before E8.5.

Identification of vascular defects in $Aggf1^{Geo/+}$ embryos and yolk sacs

The yolk sac is the major site where initial vasculogenesis and angiogenesis occur during early development (12). The $Aggf1^{Geo/+}$ yolk sacs and embryos were dissected at E9.5-E12.75, macroscopically examined, and compared to wild type counterparts

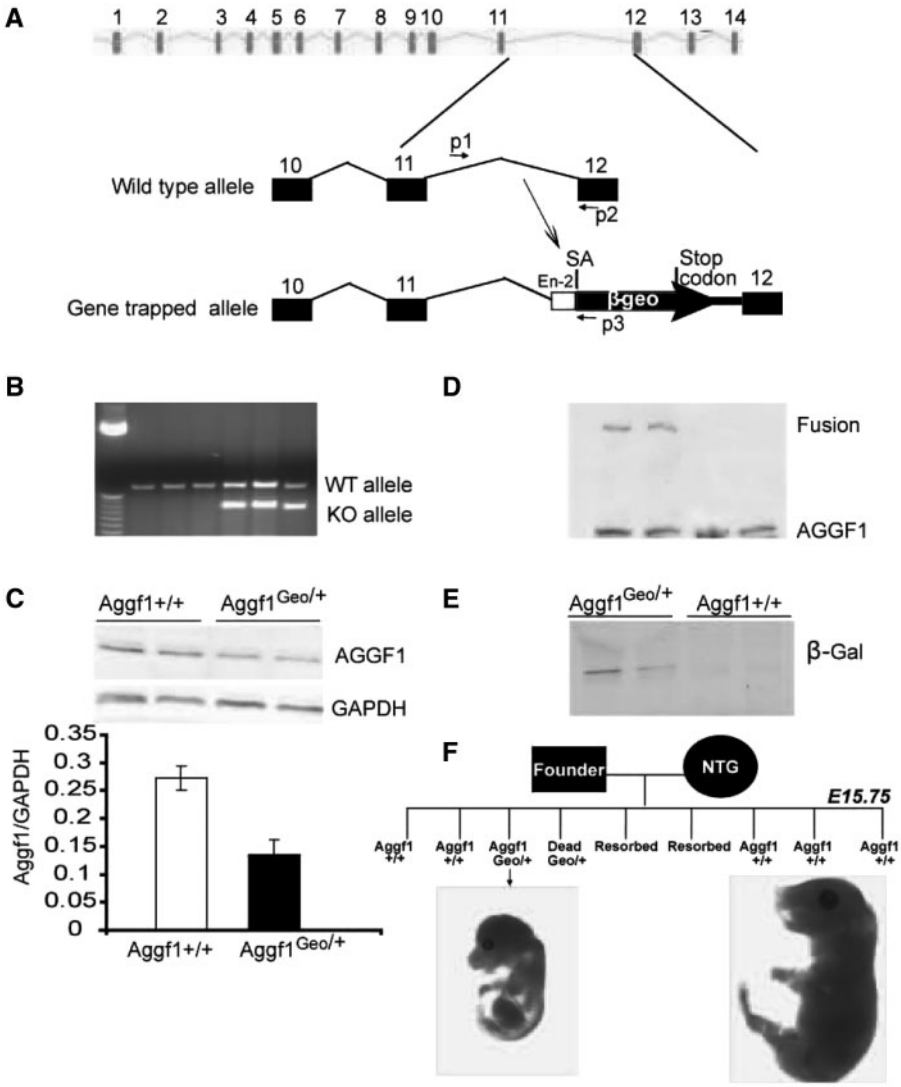

Figure 1. Generation of an *Aggf1*$^{Geo/+}$ KO mouse line using a gene-trapping strategy. (**A**) Diagram of the genomic structure of *Aggf1* showing that the *lacZ-neomycin* fusion reporter gene (*β-geo*) located downstream of an *engrailed-2* gene donor intron (*En-2*) and splice acceptor site (SA) was inserted into intron 11 of *Aggf1*. P1, P2, and P3 are PCR primers for genotyping: P1 and P2 for detecting the *Aggf1* wild type allele, and P1 and P3 for identifying the KO allele. (**B**) PCR analysis was effective in distinguishing wild type mice (P1/P2) and KO mice (P1/P3). (**C**) Western blotting analysis using an antibody against the C-terminus of AGGF1 revealed about 2-fold reduction in the expression level of AGGF1 protein in *Aggf1*$^{Geo/+}$ embryos (E12.5). (**D**) Western blotting analysis using an antibody against the N-terminus of AGGF1 revealed the presence of the AGGF1-β-geo fusion protein in addition to the wild type AGGF1 band in *Aggf1*$^{Geo/+}$ mice. (**E**) Western blotting analysis using an antibody against β-Gal detected the AGGF1-β-Geo fusion protein expression only in samples obtained from *Aggf1*$^{Geo/+}$ mice. (**F**) Detection of heterozygous lethality of *Aggf1*$^{Geo/+}$ embryos by genotyping analysis of embryos derived from breeding a chimerical *Aggf1*$^{Geo/+}$ founder mouse to a wild type mouse.

(Fig. 2). Overall, wild-type yolk sacs had extensive well-developed vasculature with large vessels and abundant vascular branching and remodeling, whereas heterozygous *Aggf1*$^{Geo/+}$ yolk sacs had fewer vessels, and much less vascular branching (Fig. 2A, left panel). Identical findings were made in *Aggf1*$^{Geo/+}$ embryos (Fig. 2A, right panel). An extensive network of vessels is present in the head, brain areas and other parts in wild-type embryos, but much fewer vessels were observed in *Aggf1*$^{Geo/+}$ embryos (Fig. 2A right panel). These results indicate that *Aggf1* is required for embryonic vascular development and angiogenesis. The abnormal vascular phenotype was detected in about 43.9% of *Aggf1*$^{Geo/+}$ KO mice. The rest of 56.1% of embryos were indistinguishable from wild type littermates, and may represent those that did survive to birth and adulthood. Hematoxylin and eosin (H&E)-stained sections of hearts at E14.5 embryos or from 8-week-old adult mice did not show apparent developmental abnormalities in *Aggf1*$^{Geo/+}$ KO mice compared with wild type mice (Supplementary Material, Fig. S1).

Whole-mount immunostaining analysis with a pan-vessel-specific marker CD31 was performed to further characterize the vascular defects in *Aggf1*$^{Geo/+}$ embryos in detail. As shown in Fig. 2B, well-developed vasculature was evident in E10.5 wild type embryos, in particularly in the brain area, but not in the same stage *Aggf1*$^{Geo/+}$ embryos. Similar defects were detected in the embryos at other developmental stage (data not shown). Interestingly, some *Aggf1*$^{Geo/+}$ embryos exhibited severe haemorrhages, especially in the cranial region (Fig. 2C and D, yellow arrows). When the embryos were stained for the expression of the *β-geo* reporter gene activity, a higher level of β-Gal expression was evident in the cranial and dorsal regions of the *Aggf1*$^{Geo/+}$ embryos compared to that of the wild type embryos (Fig. 2D), consistent with the prominent vascular defects observed in these regions.

Table 1. Heterozygous *Aggf1* KO mice show partial haploinsufficient lethality during embryogenesis

A. Genotyping analysis of E10 embryos from gene-trapping KO $Aggf1^{Geo/+}$ intercrosses

Number of litter	Number of mice	Genotype		
35	220	$Aggf1^{+/+}$	$Aggf1^{Geo/+}$	$Aggf1^{Geo/Geo}$
		94	126	0
Actual ratio		1	1.34	0
Expected Mendelian ratio		1	2	1

B. Genotyping analysis of E10 embryos from classical KO $Aggf1^{+/-}$ intercrosses

Number of Litter	Number of mice	Genotype		
23	149	$Aggf1^{+/+}$	$Aggf1^{+/-}$	$Aggf1^{-/-}$
		62	87	0
Actual ratio		1	1.40	0
Expected Mendelian ratio		1	2	1

Identification of reduce vessel density, haemorrhages and increased vascular permeability in adult $Aggf1^{Geo/+}$ KO mice

$Aggf1^{Geo/+}$ KO mice that survive to birth (56.1%) can develop into adulthood and did not exhibit obvious macroscopically abnormal phenotypes compared with wild type littermate controls. However, $Aggf1^{Geo/+}$ mice older than 40 weeks of age displayed signs of fatigue with a slightly increased rate of sudden death events, which are similar to the observation made in endothelial KO of $VEGF^{ECKO}$ mice (13). H&E-stained sections of the lungs showed leakage of blood cells (Fig. 3A). Immunosta ining analysis with a pan-vessel-specific marker CD31 showed significantly less vessel density in $Aggf1^{Geo/+}$ organs (lungs) than in wild type mice (Fig. 3A). Moreover, haemorrhages were observed in the brain, spleen and lungs of about 35% of adult $Aggf1^{Geo/+}$ mice (Fig. 3B), but never in age and sex-matched wild type littermates.

To explore the integrity of the vasculature in adult $Aggf1^{Geo/+}$ mice, vascular permeability analysis was carried out in mice at the age of 50–60 weeks by intravenous injection of Evans blue dye followed by stimulation with inflammatory mustard oil. Significantly increased extravasation into the rear footpads and ears was invariably detected in $Aggf1^{Geo/+}$ mice compared to that from wild type littermates (Fig. 3C). Vascular permeability was 2-fold greater in $Aggf1^{Geo/+}$ mice than in wild type littermates (Fig. 3C). These results suggest that the integrity of the vasculature is significantly compromised in $Aggf1^{Geo/+}$ mice, and that *Aggf1* is required for the maintenance of vascular integrity.

Molecular mechanism by which AGGF1 regulates vascular permeability

To identify the molecular mechanism underlying the compromised vascular integrity in $Aggf1^{Geo/+}$ mice, we studied VE-cadherin, which is one of the most important components of endothelial cell-to-cell adherent junctions, plays a key role in the maintenance of vascular integrity and controls vascular permeability in the adult mice (14). Thus, we analysed the phosphorylation level of VE-cadherin in isolated microvascular endothelial cells (MECs) from lungs of mutant and WT mice. MECs were isolated from $Aggf1^{Geo/+}$ mice and wild type littermates at 20-30 weeks of age, and used for Western blot analysis of phosphorylated VE-cadherin. As shown in Fig. 3D, the level of phosphorylated VE-cadherin was significantly increased in $Aggf1^{Geo/+}$ MECs compared with WT MECs. Increased phosphorylation of VE-cadherin promotes the internalization of VE-cadherin (14). Consistent with this finding, the level of VE-cadherin molecules expressed at endothelial cell membranes was decreased in $Aggf1^{Geo/+}$ mice (Fig. 3E), which can explain the compromised vascular integrity in these mice. HUVECs treated with AGGF1 showed a decreased level of phosphorylated VE-cadherin compared with cells treated with control BSA (Fig. 3F). Consequently, the level of VE-cadherin at membranes was significantly more in HUVECs treated with AGGF1 than in cells treated with control BSA (Fig. 3G). We also examined the internalization of VE-cadherin using a specific monoclonal antibody (BV6) targeting an extracellular epitope of VE- cadherin. MECs showed a cell-surface staining that was sensitive to acid wash (Fig. 3H). The internalized VE-cadherin staining signal was weak in wild type $Aggf1^{+/+}$ MECs, but markedly increased in $Aggf1^{Geo/+}$ KO MECs. This suggests that *AGGF1* haploinsufficiency increases internalization of cell surface VE-cadherin, which leads to decreased expression of VE-cadherin on cell surface and increased vascular permeability. Moreover, $Aggf1^{Geo/+}$ MECs treated with recombinant AGGF1 for 60 min showed a dramatically reduced intracellular VE-cadherin staining signal, suggesting that AGGF1 promotes cell surface localization of VE-cadherin, which is expected to decrease vascular permeability (Fig. 3H). Together, these data suggest that haploinsufficiency of *Aggf1* results in increased phosphorylation of VE-cadherin and internalization, which disrupts vascular integrity and increases vascular permeability.

AGGF1 protein blocks VE-cadherin activation and vascular permeability and significantly improves cardiac functions after ischaemia-reperfusion

As described above, AGGF1 increased VE-cadherin on plasma membranes, which is predicted to block vascular permeability. Indeed, venous administration of AGGF1 nearly eliminated the increased vascular permeability in mice undergoing reperfusion for 4 h after ischaemia (ischaemia-reperfusion or IR) compared with PBS treatment (Fig. 4A). This dramatic treatment effect is associated with the finding that AGGF1 inhibited the increased phosphorylation of VE-cadherin induced by IR compare with PBS treatment (Fig. 4B).

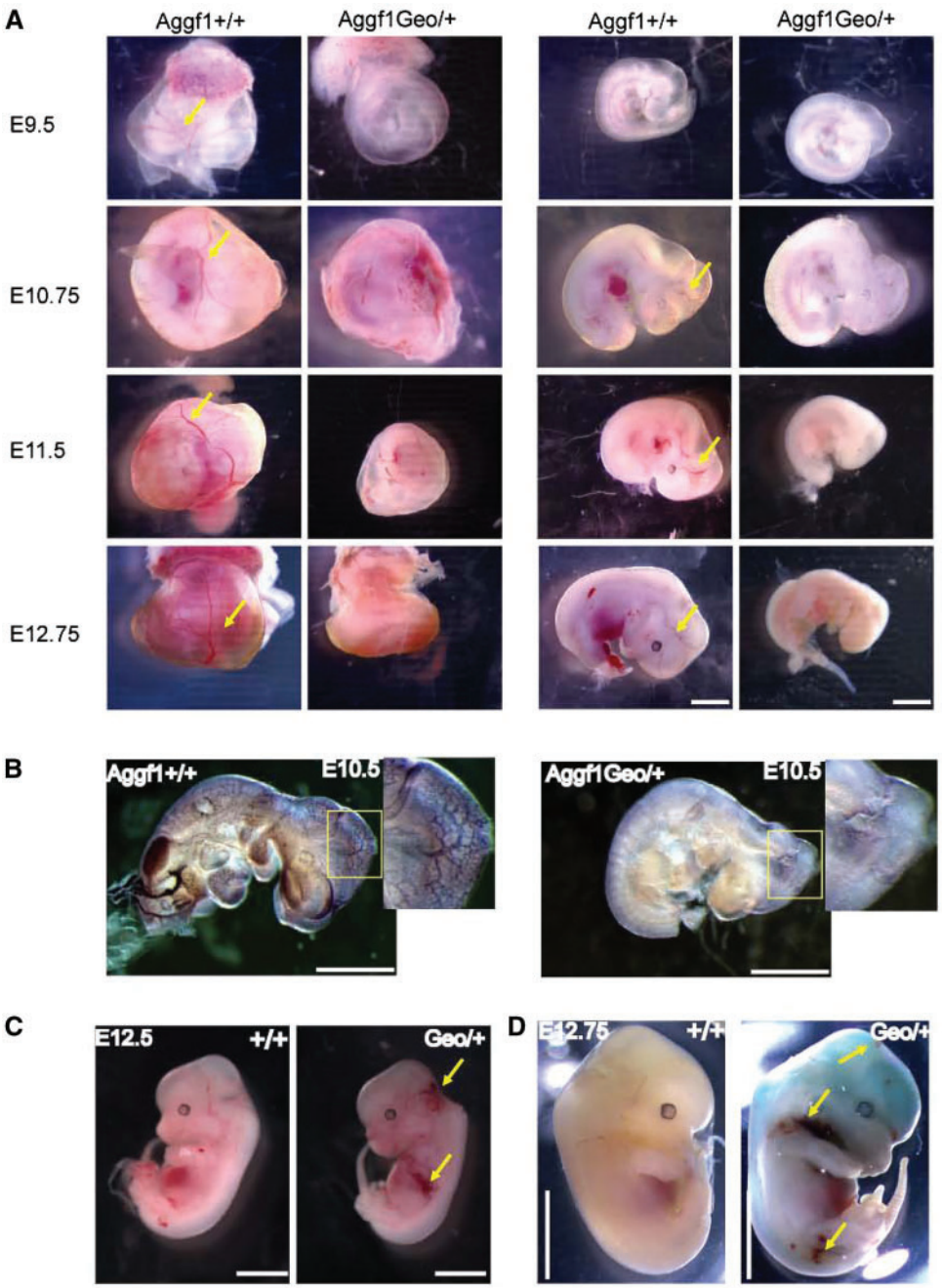

Figure 2. *Aggf1* haploinsufficiency results in defective vascular development during embryogenesis. (**A**) Images from $Aggf1^{+/+}$ and $Aggf1^{Geo/+}$ yolk sacs (left panel) and embryos (right panel) at different development stages of E9.5 to E12.75. Blood vessels are clearly visible with the red colour of blood. Note that 43.9% of *Aggf1*Geo/+ KO embryos showed the abnormal vascular phenotype, whereas the rest of 56.1% of embryos was indistinguishable from wild type embryos (data not shown). (**B**) Whole mount immunostaining for PECAM-1 (CD31) in $Aggf1^{+/+}$ and $Aggf1^{Geo/+}$ embryos at E10.5. (**C**) Haemorrhages are frequently observed in $Aggf1^{Geo/+}$ embryos and marked with yellow arrows. (**D**) Whole mount staining for β-Gal revealed a high expression level of *Aggf1* in the cranial and dorsal regions. Haemorrhages are indicated by yellow arrows. Scale bar = 300 μm.

Increased vascular permeability in IR is one of the causes for no-reflow in many patients who are treated for coronary artery disease (CAD) and myocardial infarction (MI). No-reflow is associated with a worsened prognosis and higher mortality. Because AGGF1 blocks vascular permeability, therefore, we tested whether AGGF1 can be used for therapy for IR. AGGF1 treatment significantly improved cardiac functions after IR by restoring LVEF and LVFS to nearly normal levels (Fig. 4C). Masson trichrome staining showed that the IR injury increased cardiac fibrosis and infarct sizes in the left ventricle (Fig. 4D), but AGGF1 protein therapy decreased IR-induced fibrosis (Fig. 4D) and the infarct size (Fig. 4D). Figure 4E shows the amplified images in 4D. AGGF1 significantly reduced necrosis, haemorrhages, and edema (Fig. 4F) and increased macrophage density (CD45-postive cells) associated with 3-day IR (Fig. 4G and H). These data establish AGGF1 as an effective, targeted therapy for IR injury.

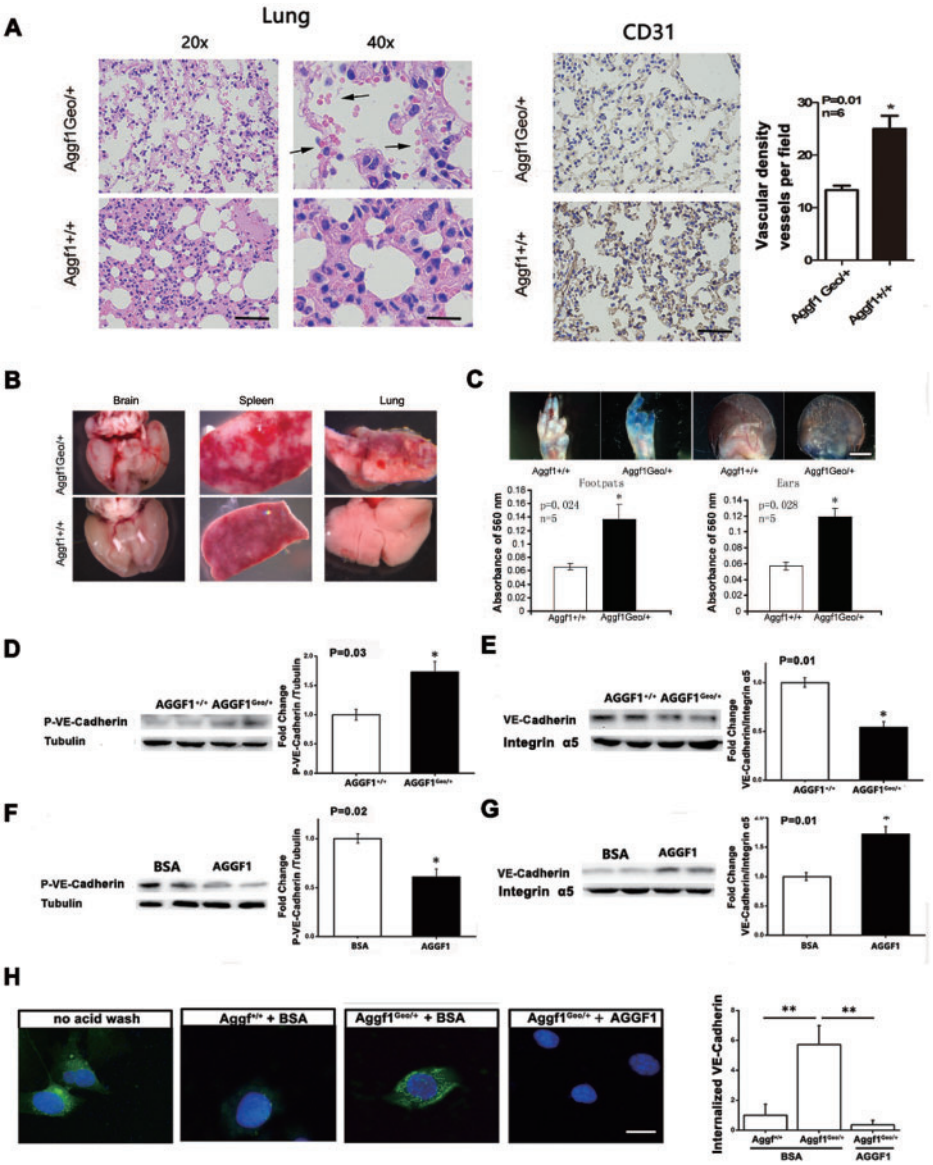

Figure 3. *Aggf1* haploinsufficiency results in vascular defects and increases vascular permeability in *Aggf1*$^{Geo/+}$ KO mice by regulating VE-cadherin phosphorylation and membrane localization. (**A**) Hematoxylin and eosin-stained sections of lungs showed leakage of blood cells *Aggf1*$^{Geo/+}$ mice but not in wild type control mice (left panel; scale bar = 100/50 μm). The right panel shows immunostaining analysis with a pan-vessel-specific marker CD31 and showed significantly less vessel density in *Aggf1*$^{Geo/+}$ organs (lungs) than in wild type mice (scale bar = 100 μm). (**B**) Macroscopic examinations of the brain, spleen and lungs identified haemorrhages in *Aggf1*$^{Geo/+}$ mice older than 32 weeks of age, but not in age-matched *Aggf1*$^{+/+}$ mice (scale bar = 2 mm). (**C**) Vascular permeability assays revealed significantly increased vascular permeability in *Aggf1*$^{Geo/+}$ mice compared to age-matched *Aggf1*$^{+/+}$ control mice at the age of 50-60 weeks. Top panels are images of Evans blue stain (scale bar = 2 mm). Bottom panels are graphs showing the amount of Evans blue extracted from respective tissues. (**D**) Phosphorylation of VE-cadherin was increased in *Aggf1*$^{Geo/+}$ ECs compared to *Aggf1*$^{+/+}$ ECs. (**E**) The protein expression level of VE-cadherin in cellular membranes was decreased in *Aggf1*$^{Geo/+}$ ECs compared to *Aggf1*$^{+/+}$ ECs. (**F**) Phosphorylation of VE-cadherin was decreased in HUVECs treated with AGGF1 compared to control BSA. (**G**) Membrane VE-cadherin expression was increased in HUVECs treated with AGGF1 compared to control BSA. (**H**) AGGF1 decreases the internalization of cell-surface-labelled VE-cadherin. MECs were incubated with the BV6 antibody at 4 °C. VE-cadherin internalization was monitored by uptake of the BV6 antibody-labelled signal (green). The remaining cell-surface antibody was visible under a 'no acid wash ' condition (left image) and washed away with a mild acid solution (other images). Blue, DAPI staining for the nucleus. Scale bars = 20 μm.

Heterozygous *Aggf1*$^{+/-}$ KO mice with a null *Aggf1* allele display partial haploinsufficient embryonic lethality and defective vascular phenotypes similar to *Aggf1*$^{Geo/+}$ KO mice

We later developed *Aggf1*$^{+/-}$ KO mice with exons 2-11 deleted and Southern blot analysis revealed successful targeting of the endogenous *Aggf1* (Fig. 5A and B). Western blot analysis showed that as expected, the expression level of AGGF1 protein was reduced by 2-fold in *Aggf1*$^{+/-}$ KO mice than that in wild type littermates (Fig. 5C). No homozygous *Aggf1*$^{-/-}$ adult mice were recovered. A considerably lower Mendelian ratio of heterozygous *Aggf1*$^{+/-}$ KO mice was found compared to wild type *Aggf1*$^{+/+}$ littermates (1.4 observed versus expected 2.0, Table 1B),

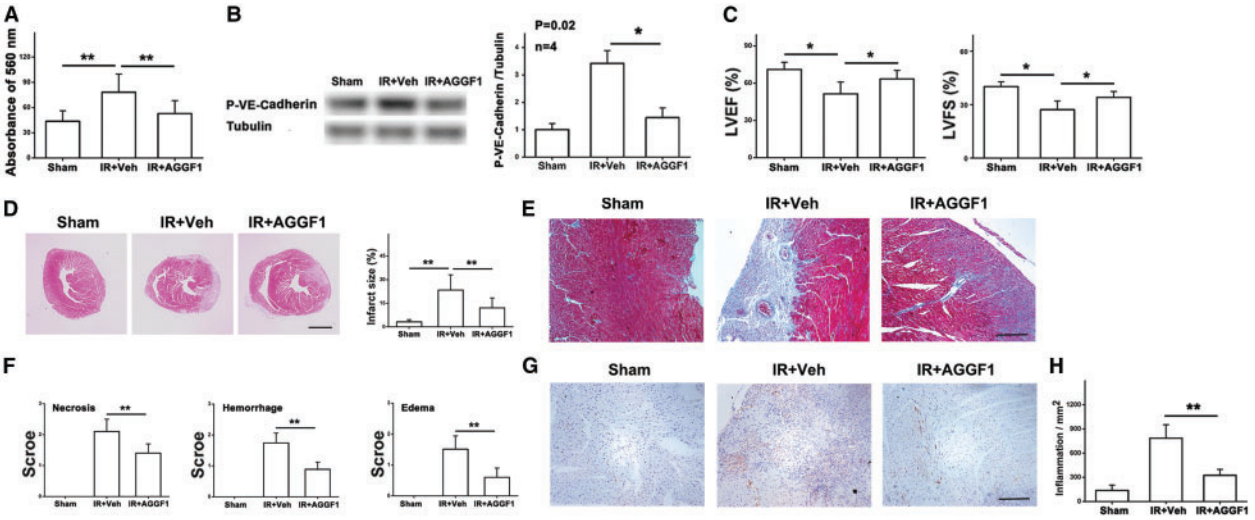

Figure 4. AGGF1 protein therapy attenuates cardiac fibrosis, decreases infarct sizes, necrosis, haemorrhages, edema, and density of macrophages induced by ischaemia-reperfusion (IR). IR injury was performed on wild type mice using a standard protocol. Mice were randomly divided into two groups to receive either vehicle or human recombinant AGGF1. Mice with sham operation were used as negative controls. (**A**) Vascular permeability assays with Evans blue dye in the hearts of mice subject to 45 min of ischaemia and 4 h of reperfusion ($n = 10$/group, $^*P < 0.05$, $^{**}P < 0.01$). AGGF1 treatment significantly inhibited the vascular leakage induced by IR. (**B**) IR-induced phosphorylation of VE-cadherin was decreased in mouse hearts after AGGF1 treatment compared with PBS treatment. (**C**) Echocardiographic data on LVEF and LVFS ($n = 10$/group, $^*P < 0.05$, $^{**}P < 0.01$). AGGF1 dramatically improved cardiac functions at 3 days after IR. (**D**) Representative images from Masson trichrome staining of cross-sections in the infarct area of hearts 3 days after IR surgery. IR mice were treated with recombinant AGGF1 protein or control PBS. AGGF1 protein therapy inhibited anterior wall fibrosis after IR. Scale bar = 1 mm. The images from Masson trichrome-stained sections in the area of infarction 3 days after IR surgery were quantified and the data are shown on the right. (**E**) Amplified images from (D). Scale bar = 100 μm. (**F**) IR-induced cardiac necrosis, haemorrhages, and edema were reduced by AGGF1 administration compared with PBS treatment. (**G**) Sections from infarcted hearts were immunostained for inflammatory cells using an anti-CD45 antibody. (**H**) The images from (G) were quantified and plotted.

indicating haploinsufficient lethality in *Aggf1*$^{+/-}$ KO mice. In addition, no homozygous *Aggf1*$^{-/-}$ embryos were identified as early as E8.5. These results further indicate that complete knockout of *Aggf1* expression is embryonically lethal before E8.5 and that haploinsufficiency of *Aggf1* causes embryonic lethality, too.

The vascular phenotypes in *Aggf1*$^{+/-}$ KO embryos and adult mice were similar to those found in *Aggf1*$^{Geo/+}$ mice. Defective vascular development was apparent in *Aggf1*$^{+/-}$ embryos and yolk sacs (Fig. 5D). Severe haemorrhages were identified in *Aggf1*$^{+/-}$ KO mice, but not in *Aggf1*$^{+/+}$ littermate controls (Fig. 5D, yellow arrows). About 35% of adult *Aggf1*$^{+/-}$ mice showed haemorrhages in the brain, lungs, and other tissues (Fig. 5E). Adult *Aggf1*$^{+/-}$ mice showed significantly increased vascular permeability (Fig. 5F). MECs from *Aggf1*$^{+/-}$ mice showed a decrease in their capability to form capillary tubes compared with that from *Aggf1*$^{+/+}$ littermates (Fig. 5G).

Identification of molecular mechanisms by which AGGF1 promotes angiogenesis and vascular development

To identify the molecular mechanisms underlying the abnormal vascular phenotypes observed in *Aggf1*$^{Geo/+}$ mutant mice, we examined the effect of AGGF1 on activation of AKT (phosphorylation on Ser473) in E12.5 embryos with the most severe vascular phenotypes. Compared to wild type embryos, the level of phosphorylated AKT was significantly reduced in *Aggf1*$^{Geo/+}$ embryos from the same litters (Fig. 6A). Similar results were obtained for *Aggf1*$^{+/-}$ KO mice (data not shown). These results suggest that AGGF1 controls vascular development by regulating the activity of AKT *in vivo*.

To confirm the *in vivo* results above, we examined whether recombinant AGGF1 protein can induce activation of AKT *in vitro*. HUVECs were allowed to adhere to AGGF1-coated wells for 5, 15, 45, 135, and 235 min. BSA-coated wells and HUVECs priori to plating were used as controls. As shown in Fig. 6B, adhesion of HUVECs to AGGF1 activated AKT. Activation of AKT started at 5 min, peaked at 15 min and gradually declined (Fig. 6B). Direct application of AGGF1 in the culture medium also activated AKT effectively (Fig. 6C). These results suggest that AGGF1 signalling involves AKT phosphorylation.

Because the studies with *Aggf1*$^{Geo/+}$ embryos could not distinguish which cells had a significant decrease of AKT activation, we performed the AKT activation study using isolated MECs from lungs of mutant and wild type mice. As shown in Fig. 6D, the expression level of the AGGF1 protein was reduced in *Aggf1*$^{Geo/+}$ MECs compared to wild type MECs, which was associated with the decreased level of phosphorylated AKT (Fig. 6E). Direct application of recombinant AGGF1 in culture media successfully rescued the decreased AKT activation in *Aggf1*$^{Geo/+}$ MECs (Fig. 6E).

To further demonstrate the critical function of AKT in AGGF1-mediated angiogenesis and vascular development, we over-expressed a constitutively active form of AKT in *Aggf1*$^{Geo/+}$ MECs and examined its effect on tube formation. MECs were isolated from *Aggf1*$^{Geo/+}$ mice and wild type littermates at 8–30 weeks of age, and used for matrigel capillary vessel tube formation. As shown in Fig. 6F, the capillary tubes formed by *Aggf1*$^{Geo/+}$ MECs were not well-connected and the number of the mature and well-connected tubes formed by *Aggf1*$^{Geo/+}$ MECs was significantly lower than that by the wild type MECs. These results suggest that the reduced capability of *Aggf1*$^{Geo/+}$ MECs to form capillary tubes may be a cause for abnormal vascular development

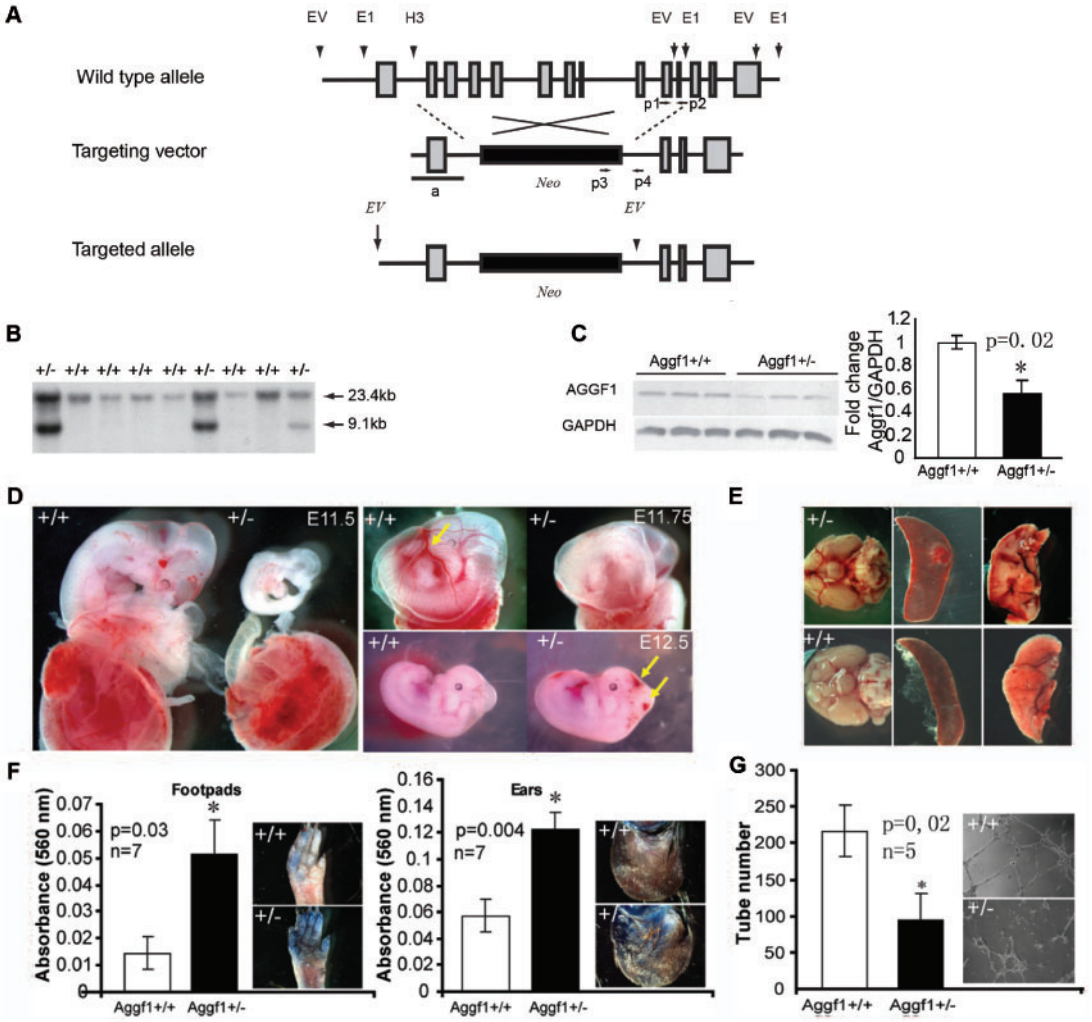

Figure 5. *Aggf1* haploinsufficiency results in vascular defects and increases vascular permeability in *Aggf1*$^{+/-}$ KO mice. (**A**) Strategy for developing a classical KO mouse line targeting *Aggf1* by homologous recombination. The wild type allele represents the genomic organization of the mouse *Aggf1* gene. The vertical gray colour-filled boxes indicate the exons of *Aggf1*. EV, E1, and H1 stand for restriction enzymes *EcoR* V, *EcoR* 1 and *Hind* 3, respectively. The targeting vector was built on pGT-N38 with insertions of the E1-H3 and the E1-E1 (3-end) fragments as the left and right arm, respectively. The horizontal black line (a) represents a probe used for Southern blotting analysis. The targeted allele shows the genomic organization of *Aggf1* after exons 2-11 are replaced with *Neo*. PCR analysis was later developed for genotyping KO mice. The positions of PCR primers for genotyping are indicated as P1, P2 and P3, P4. (**B**) Southern blot analysis was performed to detect the correctly targeted ES cell clones. The genomic DNA from the targeted ES cells produces two bands of 23.4 kb and 9.1 kb, whereas non-targeted ES cells produce a single band of 23.4 kb. (**C**) Western blotting analysis using an antibody against AGGF1 revealed about 50% reduction of AGGF1 expression in heterozygous *Aggf1*$^{+/-}$ embryos (E12.5). (**D**) Representative images showing defective vasculature in *Aggf1*$^{+/-}$ yolk sacs and embryos. Haemorrhages were also seen in 35% of developing *Aggf1*$^{+/-}$ embryos. (**E**) Detection of haemorrhages in the brain, lung and spleen of 35% of *Aggf1*$^{+/-}$ mice at 50 to 60 weeks of age. (**F**) Significantly increased vascular permeability in *Aggf1*$^{+/-}$ mice at 50 to 60 weeks of age compared to that of age-matched *Aggf1*$^{+/+}$ controls. (**G**) Matrigel-based endothelial tube formation assays revealed a decreased angiogenesis by microvascular ECs isolated from lungs of *Aggf1*$^{+/-}$ mice as compared to that from *Aggf1*$^{+/+}$ control mice at the age of 20 to 30 weeks. Scale bar = 50 μm.

in *Aggf1*$^{Geo/+}$ mice. The reduced tube formation by *Aggf1*$^{Geo/+}$ MECs was successfully rescued by overexpression of constitutively active AKT or treatment with recombinant AGGF1 (Fig. 6G). EC migration is a key process involved in angiogenesis. Similar to capillary tube formation, Wound-healing scratch assays showed that the migration of *Aggf1*$^{Geo/+}$ MECs were significantly decreased compared to *Aggf1*$^{+/+}$ MECs, but the effect was reversed by treatment with recombinant AGGF1 (Fig. 6H). These data indicate that AKT activation is responsible for AGGF1-mediated angiogenesis and vascular development.

AKT can be phosphorylated at two serine sites. In addition to Ser473, AGGF1 can also phosphorylate AKT at the Thr308 site (Fig. 6I). Interestingly, AKT activation by AGGF1 was accompanied with a decreased ERK1/2 activation level (Fig. 6I). Moreover, AGGF1 can also activate GSK3-β and p70S6K, two signalling molecules downstream of AKT (Fig. 6J).

AKT can be activated by PI3Ks, also known as phosp hatidylinositol-3-kinases (15). To identify which PI3K subunit is responsible for activation of AKT by AGGF1, we knocked each *PI3K* subunit gene down in HUVECs and then examined whether AGGF1 can still activate AKT. Among seven *PI3K* subunit genes tested, knockdown of two genes, *PIK3CA* encoding the catalytic subunit p110α and *PIK3R1* encoding the most highly expressed regulatory subunit p85α, abolished the effect of AGGF1 on activation of AKT (Fig. 7A). Consistently, the phosphorylation level of p110α and p85α subunits were significantly reduced in

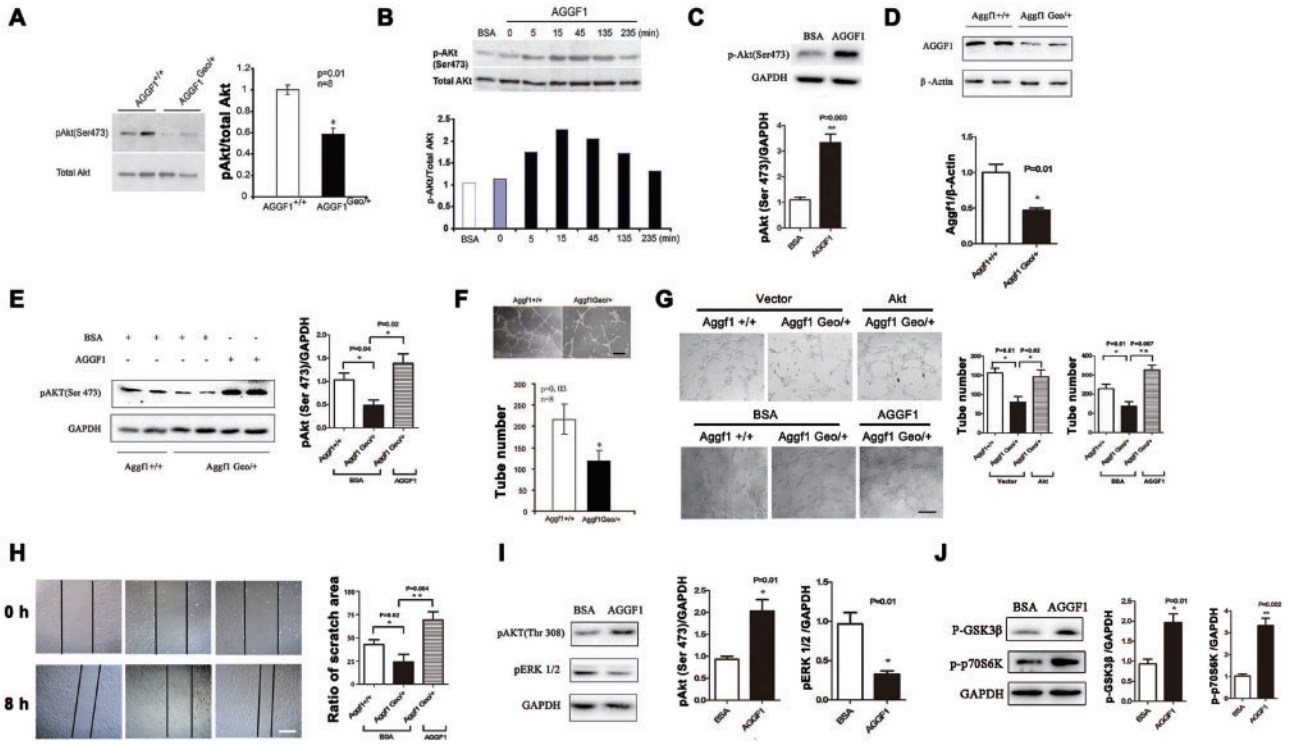

Figure 6. AGGF promotes angiogenesis and mediates vascular development by activating PI3K, AKT, GSK3-β and S6K. (**A**) *Aggf1* haploinsufficiency inhibits activation of AKT in *Aggf1*$^{Geo/+}$ KO embryos compared to wild type embryos. (**B**) Phosphorylation of AKT was induced by stimulating HUVECs with AGGF1. HUVECs were collected with EDTA dissociation buffer (Invitrogen) and plated into dishes coated with purified AGGF1 (6.4 μg/ml) or with BSA (control). Cells were allowed to attach to AGGF1 for 5, 15, 45, 135, and 235 min at 37 °C. HUVECs were then lysed in standard lysis buffer. Cell lyates were used for Western blotting analysis with indicated antibodies for phosphorylated AKT (pAkt) or total Akt. (**C**) Activation of AKT by incubating HUVECs in media containing recombinant AGGF1. (**D**) Western blotting analysis with an antibody against the C-terminus of AGGF1 revealed about 2-fold reduction of the expression level of the AGGF1 protein in microvascular ECs isolated from lungs of Aggf1$^{Geo/+}$ mice as compared to that from WT Aggf1$^{+/+}$ ECs . (**E**) Phosphorylation of AKT at Ser473 was decreased in *Aggf1*$^{Geo/+}$ ECs compared to wild type ECs, but the reduction was fully rescued by treatment of ECs with purified AGGF1 protein. (**F**) Matrigel-based endothelial tube formation assays revealed a decrease of angiogenesis by microvascular ECs isolated from lungs of *Aggf1*$^{Geo/+}$ mice as compared to that from *Aggf1*$^{+/+}$ control mice at the age of 20 to 30 weeks. Scale bar = 50 μm. (**G**) MECs from 8 week old *Aggf1*$^{Geo/+}$ mice showed reduced capillary tube formation compared with *Aggf1*$^{+/+}$ control mice, but the reduction was rescued with overexpression of constitutive active AKT or treatment with recombinant AGGF (5 μg/ml). Scale bar = 50 μm. (**H**) Reduced migration of *Aggf1*$^{Geo/+}$ MECs as compared with wild type *Aggf1*$^{+/+}$ MECs and rescue by treatment with recombinant AGGF (5 μg/ml). Scale bar = 100 μm. (**I**) Western blotting analysis revealed that AGGF1 protein (5 μg/ml) activated phosphorylation of AKT at Thr308, but decreased phosphorylation of ERK1/2. (**J**) Western blotting analysis revealed that AGGF1 protein (5 μg/ml) activated phosphorylation of GSK3-β at Ser9 and p70S6K at Thr389.

Aggf1$^{Geo/+}$ MECs compared with wild type MECs (Fig. 7B). Similarly, HUVECs treated with AGGF1 showed a significantly increased phosphorylation level of p110α or p85α (Fig. 7C). These data suggest that phosphorylation of p110α and p85α subunit is responsible for activation of AKT by AGGF1.

AGGF1 signalling is independent from VEGFA signalling in activation of AKT

Considering that both VEGF-A and AGGF1 were associated with haploinsufficiency lethality and abnormal vascular development in mice, we determined the effect of reduced *Aggf1* expression on the expression levels of *VEGF-A* and other related genes. Quantitative real-time reverse transcription PCR (RT-PCR) analysis with total RNA samples isolated from E12.5 embryos showed that the expression levels of *VEGF-A* and *VEGFR2* were not significantly different between *Aggf1*$^{Geo/+}$ and wild type control embryos (Supplementary Material, Fig. S2). Similarly, no difference was detected on expression of *eNOS*, *Cdh5* (encoding VE-cadherin), and *Hdgf* (Supplementary Material, Fig. S2). The expression levels of *Vegfr2* were not significantly different between *Aggf1*$^{Geo/+}$ ECs and wild type ECs (Supplementary Material, Fig. S3A). Similarly, no difference was detected on the expression of *AGGF1* in HUVECs treated with *VEGFR2* siRNA (Supplementary Material, Fig. S3A). These data suggest that there is no cross-regulation between *Aggf1* and *Vegfa*/*Vegfr2*.

Because both VEGFA and AGGF1 can activate AKT, we examined whether the AGGF1 pathway cross-talks with the VEGFA-VEGFR2 pathway. AGGF1 treatment did not increase the phosphorylation level of VEGFR2 at Tyr1175 in HUVECs (Supplementary Material, Fig. S3B). Phosphorylation of AKT at Ser473 was decreased in *Aggf1*$^{Geo/+}$ ECs compared to wild type ECs as described above, but VEGFA treatment (100 ng/ml) for 20 min can still activate AKT even in *Aggf1*$^{Geo/+}$ ECs (Supplementary Material, Fig. S3C). Phosphorylation of AKT at Ser473 was decreased in HUVECs transfected with *VEGFR2* siRNA compared with control scramble siRNA (Supplementary Material, Fig. S3D, BSA treatment group). AGGF1 treatment can still activate AKT even in HUVECs transfected with *VEGFR2* siRNA (Supplementary Material, Fig. S3D, AGGF1 group). These data suggest that the AGGF1 signalling pathway is independent from the VEGFA pathway in activation of AKT.

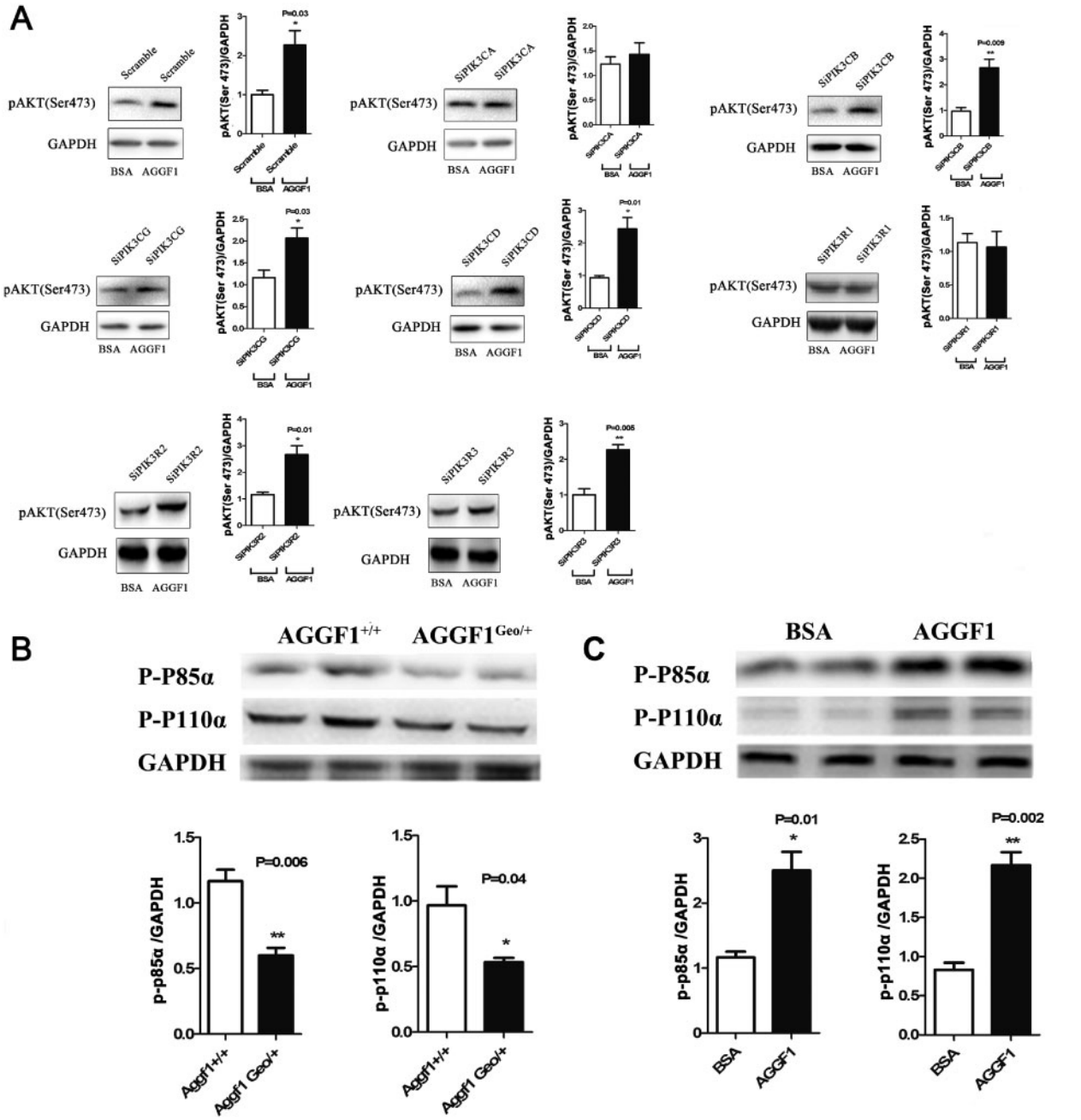

Figure 7. AGGF activates AKT by activating PI3K. (**A**) Effects of knockdown of 7 different genes encoding different PI3K subunits on AGGF1-mediated AKT activation. (**B**) Phosphorylation of P85α and p110α was decreased in *Aggf1*$^{Geo/+}$ ECs compared to *Aggf1*$^{+/+}$ ECs. (**C**) Phosphorylation of P85α and p110α was increased in HUVECs treated with AGGF1 compared to control BSA.

AGGF1 is required for pathological angiogenesis

To extend the essential role of AGGF1 in developmental angiogenesis to pathological angiogenesis, we investigated whether haploinsufficiency of *Aggf1* had any effect on tumour growth, which requires angiogenesis. As melanomas are heavily angiogenesis-dependent, we first studied the possible role of AGGF1 signalling in murine melanoma models. Two mouse melanoma cell lines, B16F10 and B16F0, were studied. Compared to wild type control mice, tumour growth for both B16F10 and B16F0 was significantly inhibited in *Aggf1*$^{Geo/+}$ mice (Fig. 8A). Tumour growth curves were constructed in an independent set of experiments (Fig. 8B), which further showed significantly reduced tumour growth in *Aggf1*$^{Geo/+}$ mice. Vascular density was quantified after immunostaining for CD31 and showed a significant decrease in tumours grown in *Aggf1*$^{Geo/+}$ KO mice (Fig. 8C). Similar observations were made in *Aggf1*$^{+/-}$ KO mice (Fig. 8D and E). These results indicate that *Aggf1* is required for tumour angiogenesis (pathologic angiogenesis) and growth.

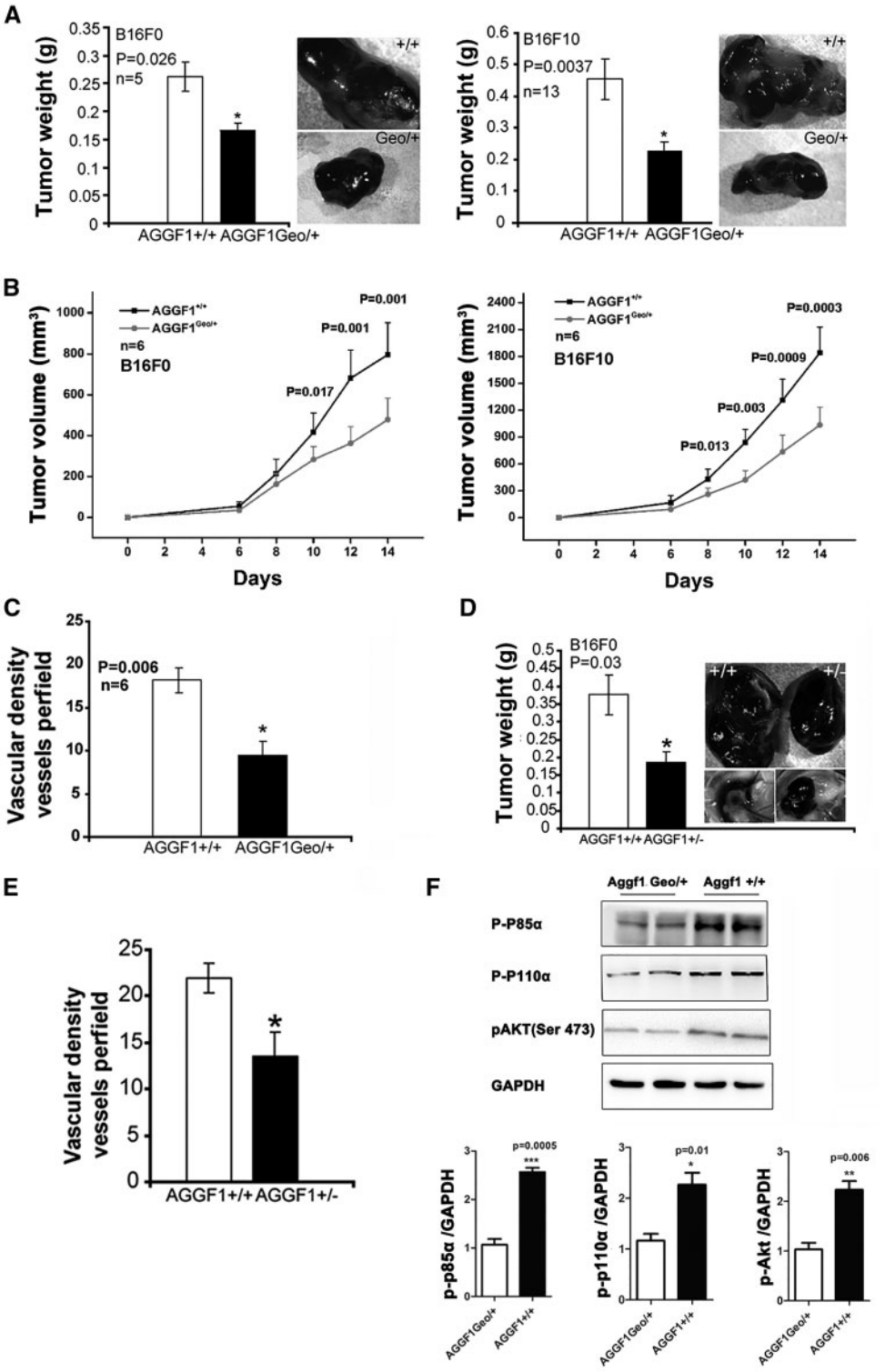

Figure 8. *Aggf1* haploinsufficiency inhibits tumor angiogenesis and growth. (**A**) The weight of subcutaneous tumors grown in mice. Both murine melanoma B16F0 (left) and B16F10 tumor weight (right) was significantly reduced in $Aggf1^{Geo/+}$ mice as compared to $Aggf1^{+/+}$ controls. (**B**) Growth curves for B16F0 and B16F10 tumors in $Aggf1^{Geo/+}$ and $Aggf1^{+/+}$ mice. (**C**) CD31 staining revealed significantly reduced blood vessel density in tumors grown in $Aggf1^{Geo/+}$ mice compared to that from $Aggf1^{+/+}$ controls. (**D-E**) Identical results as in (A) and (C) from gene-trapping $Aggf1^{Geo/+}$ KO mice were found for classical $Aggf1^{+/-}$ KO mice. (**F**) Western blot analysis for p-P110α, p-P85α, and pAKT with protein extracts from tumors from $Aggf1^{Geo/+}$ mice and $Aggf1^{+/+}$ controls.

Tumours were excised and used for Western blot analysis for activation of PI3K and AKT. The levels of p-P85α, p-P110α and pAKT were all significantly reduced in solid tumours from $Aggf1^{Geo/+}$ KO mice as compared to that from wild type mice (Fig. 8F). The data suggest that similar to physiological angiogenesis, AGGF1-mediated AKT activation is also involved in pathological tumour angiogenesis.

Discussion

Haploinsufficient lethality of *Aggf1* KO mice

The haploinsufficient lethality of *Aggf1* was surprising because such a phenotype has been identified only for two other genes to date, including *VEGF-A* (16,17) and the endothelial Notch ligand Delta-like 4 (*Dll4*) (18–20). To the best of our knowledge, *Aggf1* is the third gene for which genetic ablation causes heterozygous lethality. Both *VEGF-A* and *Dll4* play critical roles in vascular development, and the finding of haploinsufficient lethality of *Aggf1* is consistent with its essential role in vascular development. The reason of embryonic lethality in the homozygous *Aggf1* KO mice is unknown. We have demonstrated previously that in zebrafish, *Aggf1* is the earliest molecular determinant for mesodermal differentiation to hemangioblasts, which are multipotent stem cells for the development of vascular and blood cells (11). Therefore, a complete deficiency of *Aggf1* may affect stem cell differentiation and the earliest developmental events, resulting in early embryonic lethality. The heterozygous lethal phenotype may differ from the homozygous lethality in *Aggf1* KO mice because severe haemorrhages in early stage heterozygous embryos (Fig. 2C) may be one of the causes for lethality.

Aggf1 is involved in maintaining vascular integrity by regulating VE-cadherin

Heterozygous *Aggf1* KO mice exhibited frequently impaired vasculature development in yolk sacs and embryos (Figs 2 and 5). In addition to embryos, vascular defects were also observed in adult heterozygous KO mice. Haemorrhages were noted in 35% of adult heterozygous KO mice (Fig. 3), suggesting that *Aggf1* is crucially involved in the maintenance of vascular functions, including vascular integrity and stability. This notion was supported by the observation that adult heterozygous KO mice displayed significantly increased vascular permeability (Figs 3 and 5). Moreover, lung MECs from heterozygous KO mice were defective in capillary tube formation in an *in vitro* matrigel angiogenesis assay, which was rescued by AGGF1 provided in the medium (Fig. 6). These results provide *in vivo* evidence that *Aggf1* has an essential role in the maintenance of vascular integrity. Mechanistically, increased phosphorylation of VE-cadherin and its decreased membrane localization are responsible for comprised vascular integrity in *Aggf1* KO mice (Fig. 3).

VEGFA was tried for therapeutic angiogenesis in the treatment of cardiovascular diseases, but presented with a severe side effect of increased vascular permeability, leading to no-reflow (21). Inadequate myocardial perfusion due to no-reflow occurs in 30% of patients under treatment for coronary artery disease (CAD) and myocardial infarction (MI), and has been linked to a worse prognosis and a higher risk of death (22). Increased vascular permeability and no-reflow limit the utility of VEGFA in treatment of cardiovascular diseases. In this study, we found that vascular permeability was increased in *Aggf1* KO mice and AGGF1 protein can block vascular permeability induced by IR in mice. We further demonstrated that AGGF1 was effective in treating ischaemia-reperfusion by blocking vascular permeability via inhibiting phosphorylation of VE-cadherin. Due to the property of AGGF1 in inhibition of vascular permeability, AGGF1 becomes a better tool than VEGFA in treatment of cardiovascular diseases.

AGGF1 is involved in tumour angiogenesis and growth

Recent clinical trials with a combination of bevacizumab, an anti-VEGF-A antibody, with chemotherapy, produced encouraging response in several types of tumours. However, more than 50% of patients do not respond to bevacizumab antiangiogenic treatment (23). Furthermore, the duration of response is modest and highly variable among different patients. Resistance to the bevacizumab antiangiogenic therapy is also an issue. The tumour vasculature is highly heterogeneous (24). We investigated the potential role of AGGF1 signalling during tumour angiogenesis, and found that tumour growth of melanoma tumours and accompanied angiogenesis were significantly reduced in heterozygous *Aggf1* KO mice compared to wild-type mice (Fig. 8). These results strongly suggest that AGGF1 is required for pathologic tumour angiogenesis, and that AGGF1 may be a novel target for developing alternative or complementary anti-angiogenic therapies to anti-VEGF therapy.

The AGGF1-PI3K-AKT signalling axis and the pathogenesis of KTS

Our data in cultured HUVECs, isolated lung MECs from mice, and KO embryos indicate that AGGF1 regulates angiogenesis and vascular development by activating AKT (Fig. 6). Further analysis showed that phosphorylation of p110α and p85α PI3K subunits was responsible for activation of AKT by AGGF1 (Fig. 7). These data indicate that PI3K-AKT is a critical molecular signalling pathway downstream of AGGF1 action.

We previously showed that increased AGGF1 expression is the cause of KTS (6,7), which is consistent with histologic analysis of subcutaneous veins in 33 KTS patients showing an increase in the number of small venules in affected KTS tissues (25). As overexpression of AGGF1 expression increases phosphorylation of the p110α catalytic subunit of PI3K and p85α regulatory subunits of PI3K, leading to activation of AKT (Fig. 7), we suggest that the AGGF1-PI3K-AKT signalling axis plays a role in the pathogenesis of KTS. Recently, somatic mutations in *PIK3CA* (encoding the p110α catalytic subunit) were identified in tissue samples from KTS patients (26,27). Our data mechanistically link two KTS genes, *AGGF1* and *PIK3CA*, together and further support our hypothesis that the pathogenesis of KTS involves the AGGF1-PI3K-AKT signalling pathway. Future studies are needed to validate the hypothesis and further elucidated the detailed molecular mechanisms for the pathogenesis of KTS.

Limitations

(1) The present study focused on the function of *Aggf1* in ECs. Future studies with EC-specific or VSMC-specific *Aggf1* KO mice are expected to identify cell specific roles of *Aggf1*. (2) The molecular mechanism by which AGGF1 activates PI3K remains to be identified. (3) There are three forms of AKT kinases, i.e. AKT1, AKT2, and AKT3. Our data could not distinguish which AKT isoform is responsible for the AGGF1 function because the most commercial phosphor-AKT antibodies recognize all three isoforms. However, based on published data, AKT1 may be the most likely candidate isoform responsible for AGGF1 signalling. Chen *et al.* (28) showed that AKT1 was the predominant AKT isoform in vascular cells and *Akt1*$^{-/-}$ knockout mice showed increased vascular permeability as observed in heterozygous *Aggf1* KO mice. Lee *et al.* (29) recently showed that endothelial *Akt1*, but not *Akt2*, is critical for vascular development and function. *Akt3* expression was found only in the testes and brain (30)

but its role in vascular development was not reported. (4) The phenotype of *Aggf1* KO mice was more severe than that from *Akt* KO mice. No homozygous *Aggf1* KO embryos were ever found, and 43.9% of heterozygous *Aggf1*$^{Geo/+}$ embryos died before birth. Global deletion of all three *Akt* isoforms was early embryonic lethal, however, *Akt1*$^{+/-}$/*Akt2*$^{-/-}$/*Akt3*$^{-/-}$ mice are viable and develop normally without obvious defects (31). Thus, AKT activation may not be the sole signalling pathway downstream of AGGF1 function. This is supported by our findings that AGGF1 can mediate phosphorylation of VE-cadherin as well as ERK1/2 (Figs 3 and 6). There may be additional signalling pathways for AGGF1 action that remain to be identified.

Conclusions

The results of this study demonstrate that *Aggf1*, the first gene associated with vascular disease KTS, is essential for both developmental angiogenesis and pathological tumour angiogenesis/growth. Both *in vitro* and *in vivo* data suggest that AGGF1 promotes angiogenesis and vascular development by activating PI3K and AKT. Our data also indicate that *Aggf1* is required for maintenance of vascular integrity by regulating phosphorylation and membrane localization of VE-cadherin. This study establishes AGGF1 as a novel target for both therapy of IR and antiangiogenic therapy and suggests that AGGF1-PI3K-AKT signalling is a key for the pathogenesis of KTS.

Materials and Methods

Generation and genotyping of *Aggf1*$^{Geo/+}$ knockout mice

To characterize the physiological function of *Aggf1*, we generated two lines of heterozygous knockout (KO) mice for *Aggf1*: one gene-trapping KO line with the G-patch domain and C-terminus of AGGF1 deleted (*Aggf1*$^{Geo/+}$), and the other classical KO line with exons 2 to 11 deleted (*Aggf1*$^{+/-}$).

The *Aggf1*$^{Geo/+}$ mice were created using a gene-trapping embryonic stem (ES) cell line PT036, which was identified from the BayGenomics database (http://baygenomics.ucsf.edu/). We had the PT036 ES cell line recovered and re-sequenced to confirm its identity. PCR analysis with a series of primer pairs covering the entire *Aggf1* gene was used to define the precise insertion point of the gene-trapping vector, which contains a splicing adaptor followed by a *β-geo* reporter gene (Fig. 1A). The gene-trapping vector was inserted into intron 11 of *Aggf1*, which results in a truncated AGGF1 protein with the G-patch domain and C-terminus replaced with β-Geo (Fig. 1). This results in the production of a fusion protein with 569 N-terminal amino acids of AGGF1 fused to 1,327 amino acids of the β-galactosidase-neomycin (β-geo) protein (an estimated molecular weight of 212 kDa). The Bay Genomics/University of California at Davis Facility performed blastocyst injection of the ES cells (in a mixed genetic background of C57BL6/129Sv), which yielded 14 chimeras (11 males and 3 females). Breeding of chimerical mice to wild type C57BL/6 mice generated successful germline transmission, yielding F1 mice heterozygous for the modified *Aggf1* allele (hereafter referred to as *Aggf1*$^{Geo/+}$ mice). Sibling matings between *Aggf1*$^{Geo/+}$ mice failed to generate any homozygous *Aggf1*$^{Geo/Geo}$ mice.

We developed a PCR-based method for genotyping *Aggf1*$^{Geo/+}$ mice. *Aggf1*$^{Geo/+}$ mice can be genotyped by PCR analysis using primers shown in Fig. 1A. The wild type allele in *Aggf1*$^{Geo/+}$ mice can be detected by the presence of a PCR band of 865 bp generated by PCR analysis using forward primer 5'- TGC AGT CTT ATA GTG GAG TGC- 3' and reverse primer 5'- TCA TCT CTT TGG AAA GTC CCT TCG -3'. The mutant allele can be identified by the presence of a 669 bp band using forward primer 5'- TGC AGT CTT ATA GTG GAG TGC- 3' and reverse primer Rev 5'- TTC ACT GAG TCT CTG GCA TCT C -3' (669 bp PCR product). Mouse genomic DNA was isolated using standard methods as described (32–34). Standard PCR conditions were used as described (32–34). The PCR program consists of denaturation at 95°C for 5 min, 35 cycles of 95°C for 30 s, 58°C for 30 s and 72°C for 45 s, and 72°C for 10 min, followed by storing at 4°C.

Animal protocols performed in this study were approved by the Institutional Animal Care and Use Committee (IACUC) at Cleveland Clinic and Huazhong University of Science and Technology.

Generation and genotyping of *Aggf1*$^{+/-}$ KO mice

For generation of classical *Aggf1*$^{+/-}$ KO mice, we constructed a targeting vector that could produce a null allele for *Aggf1* by homologous recombination. The targeting vector has exons 2-11 of *Aggf1* deleted and replaced with the neomycin-resistance (*Neo*) gene. Positive ES cells with correct targeting of *Aggf1* were identified by Southern blotting analysis.

The targeting vector was electroporated into mouse ES cells in a mixed genetic background of C57BL6/129Sv. ES cells were cultured as described previously (35). Genomic DNA was isolated from ES cells using standard methods as described (35) and used for Southern blotting. The probe for Southern blotting, a 780 bp genomic fragment from the mouse *Aggf1* gene, was generated by PCR analysis using genomic DNA from normal C57BL/6 mice, forward primer 5′- TGG AGA TGG GGT GGA AAC G -3′ and reverse primer 5′- TGT GTC CGT CGA AGC TGA AGC TG-3′. The identity of the probe was confirmed by DNA sequencing analysis.

Southern blotting was performed as described (32,33). In brief, ES cell DNA samples were digested with *Eco*R V (Invitrogen), separated on a 0.8% agarose gel and transferred to a Hybond N+ membrane (Amersham). The membrane was prehybridized at 65 °C for 60 min with hybridization buffer (Amersham™ Rapid-Hyb Buffer). The probe was labelled with -^{32}P-dCTP using the Prime-It II Random Primer labeling system (Stratagene), purified with Sephadex G-50 column (Roche) and added to the hybridization buffer for 5 h. The membrane was washed twice with 2 SSC/0.1% SDS at 65 °C for 30 min and for two times with 0.5 SSC/0.1% SDS at 65 °C for 30 min and with 0.1 SSC/0.1% SDS at 65 °C for 30 min. The membrane was then exposed to X-ray film. We analysed 259 embryonic stem (ES) cell clones and found that seven of them were correctly targeted. Two targeted ES clones were injected into blastocysts from C57BL/6 mice. The injection yielded three positive chimeras. Breeding of chimerical mice to wild type C57BL/6 mice generated successful germline transmission, yielding F1 mice heterozygous for *Aggf1* null allele (hereafter referred to as *Aggf1*$^{+/-}$ mice). Brother-sister matings between *Aggf1*$^{+/-}$ mice failed to generate any homozygous *Aggf1*$^{-/-}$ mice.

We developed a PCR-based strategy to genotype *Aggf1*$^{+/-}$ KO mice. The wild type allele can be distinguished by PCR analysis using forward primer 5-GAG CTC ACC TCC GCC TCG AT-3 and reverse primer 5-CCT CCT TAC TTA GTG CTG GAC-3, which yields a 784 bp PCR product. PCR primers for detecting the KO allele are 5-TAT AGA TCT CTC GTG GGA TCA TT-3 (forward) and 5-GAA TGG TCT GAG CCA TGT AGT GTT-3 (reverse) and generate a 309 bp PCR product. The PCR conditions and programs are identical to that for genotyping *Aggf1*$^{Geo/+}$ mice as described above.

Isolation and CD31 (PECAM-1) immunostaining of mouse embryos

Successful mating was monitored by the presence of a vaginal plug, a time point referred to as 0.5 dpc. Pregnant females were sacrificed at different time points and embryos were dissected from the uterus for further characterization. The embryos were photographed directly to examine their gross morphology. The development of vascular structure at different embryonic stages can be studied because the vessels are filled with red blood, whereas other parts are transparent.

Whole-mount CD31- or PECAM-1 staining was used to further characterize the development of vascular structure in embryos and performed as described (6). Mouse embryos were isolated, rinsed using ice-cold phosphate-buffered saline (PBS) for 10 min, fixed in 4% paraformaldehyde/PBS at 4 °C overnight, rinsed 3 times for 5 min in PBS at room temperature, dehydrated in a series of methanol (25%, 50%, 75%, 100%) at room temperature, subsequently bleached with 5% hydrogen peroxide in methanol for 4–5 h at room temperature, and washed three times in 100% methanol. The embryos were rehydrated through 75%, 50%, 25% of methanol and PBS at room temperature, then incubated in PBSMT (3% dried milk, 0.1% Triton X-100, PBS) twice for 1 h at room temperature, and stained overnight at 4 °C with an anti-PECAM1 antibody (clone MEC 13.3, Pharmingen) diluted 1:50 in PBSMT. The embryos were then washed in PBSMT at 4 °C five times (1 h each), followed by incubation with a HRP-conjugated secondary antibody (goat anti-rat IgG, Jackson, 1:200 dilution) in PBSMT at 4 °C overnight. The embryos were then rinsed in PBSMT at 4 °C five times (1 h each), in PBT (0.2% BSA, 0.1% Triton X-100, PBS) for 20 min at room temperature, and then incubated in the developing solution (0.3 mg/ml DAB, 0.5% $NiCl_2$ in PBT) for 20 min at room temperature. H_2O_2 was added to a final concentration of 0.03% and the incubation continued for 10 min at room temperature for the colour to develop. Finally, the stained embryos were washed in PBS and fixed in 2% paraformaldehyde plus 0.1% glutaraldehyde in PBS at 4 °C overnight, examined under a microscope and photographed (LEICA EC3 digital camera, Switzerland).

Immunohistochemical staining of whole mouse embryos for β-galactosidase

To examine *lacZ* expression, *Aggf1*$^{Geo/+}$ mouse embryos at different developmental stages were dissected out of the uterus, rinsed with 100 nM sodium phosphate (pH 7.3) buffer, fixed in 2% paraformaldehyde and 0.2% glutaraldehyde/PBS for 30 min on ice with shaking, and then fixed for additional 1–4 h on ice in formalin/glutaraldehyde fixative (0.2% glutaraldehyde, 2% formalin in PBS). The embryos were washed three times for 15 min with PBS, stained overnight at 37 °C in X-gal solution (5 mM potassium ferrocyanide crystalline, 5 mM potassium ferricyanide trihydrate, 2 mM magnesium chloride, and 1 mg/ml X-gal, protected from light), washed three times for 10 min in PBS, and stored in *lacZ* wash buffer at 4 °C before photograph. All images were captured using an LEICA EC3 digital camera (Switzerland) under a dissection microscope (LEICA).

Tumour growth and angiogenesis assays

4–6 weeks old *Aggf1* heterozygous KO mice and age- and sex-matched wild type littermate control mice were given single s.c. injections of 1×10^6 B16F10 or B16F0 melanoma cells. Tumours were collected 8 days after injection. The morphology of the isolated tumours was captured using an LEICA EC3 digital camera (Switzerland) under a dissection microscope (LEICA). The tumours were fixed with formalin, embedded with paraffin, and cut into 6-μm sections. The sections were stained with H&E as previously described by us (33,36).

Immunohistochemical staining of tumour sections was carried out by using a monoclonal antibody against PECAM-1 (clone MEC 13.3, Pharmingen), a polyclonal rabbit anti-human Von Willebrand Factor (DakoCytomation), or an EPOS™ anti-human smooth muscle actin/HRP antibody (clone 1A4, DakoCytomation). The sections were counter-stained with hematoxylin (Vector), and examined under an Olympus microscope. Representative areas were photographed using an ORCA-ER digital camera (HAMAMATSU). The quantitative data for the density of blood vessels was obtained by counting the total numbers of PECAM-1 positive blood vessels across whole sections of tumours.

Vascular permeability assays

Vascular permeability assays were carried out using Evans blue dye as previously described (28,37–39). In brief, Evans blue dye (30 mg/kg in 100 μl PBS; Sigma Chemical Co., St. Louis, Missouri, USA) was injected into the tail vein of 50- to 60-week-old mice. In some experiments, mustard oil (Sigma Chemical Co.) diluted to 5% in mineral oil was applied to the dorsal and ventral surfaces of the ear with a cotton swab 1, 15 and 30 min after the injection, respectively. The respective tissues were photographed to visualize the permeability of the blue dye. The mice were then euthanized and immediately perfused via the left ventricle with 20 ml of PBS. Ears and feet were removed, blotted dry, and weighed. The Evans blue dye was extracted from equal weights of ears and feet with 1 ml of formamide overnight at 55 °C and measured spectrophotometrically at 560 nm. Other organs, including the heart, lung, spleen, an equal weight of small intestinal tissue, liver, kidney and brain, were harvested and incubated in 2 ml of formamide for 3 days to elute Evans blue dye at room temperature and measured spectrophotometrically at 560 nm.

Real-time RT-PCR analysis

Quantitative real-time reverse transcription polymerase chain reaction (RT-PCR) was carried out using the SYBR Green PCR Supermix (VWR) and primers listed in Supplementary Table S1 as described previously (40–43). The data were analysed as relative expression values as previously described (40–43). The *GAPDH* gene was used as a control to normalize the samples for comparison.

Western blotting analysis

Wild type and heterozygous embryos at the E12.5 stage (a stage with most severe phenotypes) were isolated and lysed in lysis buffer containing protease/phosphatase inhibitors (10 mM sodium fluoride, 5 mM sodium pyrophosphate, 20 mM Tris-HCl (pH 8.0), 100 mM NaCl, 1 mM EDTA, 0.5% NP-40 and 1 x protease/phosphatase cocktail solution (Roche)). A 100 μg of protein extracts was separated on SDS-PAGE gels and Western blot analysis was performed as previously described (9,44,45). Antibodies used for Western blot analysis include rabbit polyclonal antibodies against the C-terminus or N-terminus of AGGF1 made in our laboratory, GAPDH (Sigma), tubulin (Minipore), β-galactosidase (Santa Cruz Biotechnology), integrin α5 (Cell Signalling),

AKT (Cell Signalling), phosphorylated AKT (Cell Signalling), phosphorylated ERK1/2 (Cell Signalling), phosphor-VE-cadherin (Affinity), and phosphorylated PI3K catalytic subunit p110α (Bioss) and regulatory subunit p85α (Affinity). The protein signal was visualized by using the ECL detection system (Amersham Biosciences). The membranes were re-probed using an anti-GAPDH monoclonal antibody (Chemicon), which serves as the loading control. The images were scanned and quantified by densitometry (Melanie 2D gel analysis software, Millennium).

Isolation and immunostaining analysis of microvascular endothelial cells (MECs) from murine lungs

Mice were anaesthetized and sacrificed (20–30 weeks of age for the first set and 8 weeks of age for the second set). The lungs were harvested, placed in sterile ice-cold 1×PBS, chopped into pieces, and washed with a copious amount of sterile, ice-cold 1×PBS to remove a maximum amount of blood cells from the lung tissue. Lung tissues were minced using a scalpel blade in 60-mm sterile petri plates under filtered laminar airflow. The minced tissue samples were incubated with 3 mg/ml of collagenase-dispase mixture for 4 h at room temperature with gentle shaking. After 4 h, cells were isolated from the tissue fragments using a tissue strainer (CELLECTOR tissue sieve). The supernatant was collected and centrifuged at 320 g for 5 min using a Beckman Coulter centrifuge (Allegra 6 Centrifuge). The supernatant was discarded and the cell pellets were washed twice with sterile ice-cold 1×PBS. The cells were resuspended in endothelial cell growth media (DMEM with 25 mM HEPES (Invitrogen), supplemented with 10% fetal bovine serum, 90 μg/ml of heparin sulphate, 90 μg/ml of endothelial cell growth factors (BD Biosciences), 10,000 U/ml of penicillin, and 10 mg/ml of streptomycin).

MECs were then isolated from the mixture of cell population using an anti-CD31 antibody as described (46). The cells were centrifuged and resuspended in DMEM F12 medium, mixed with 100 μl of Dynabeads (Dynal MPC) and incubated at 4 °C for 15 min. The endothelial cells bound to the magnetic beads were separated by trypsin digestion. After washing, these cells were plated on to tissue culture plates precoated with 1% (w/v) gelatin or 0.01% (w/v) fibronectin.

For an immunostaining assay for internalization of VE-cadherin, isolated MECs were seeded in HUVEC growth medium in 8-well dishes 24 h prior to the experiment. Cell-surface VE-cadherin was labelled at 4 °C with the extracellular VE-cadherin domain-targeting antibody BV6 (Enzo Life Sciences) (1:200 dilution) for 60 min, rinsed with ice-cold PBS and stimulated with recombinant AGGF1 or control BSA at 37 °C for 60 min. MECs were then subjected to a mild acid wash. Subsequently, cells were fixed and stained using an anti-mouse Alexa Fluor-coupled secondary antibody (Life Technologies). Nuclei were counterstained using DAPI (Carl Roth). Images were captured under a fluorescent microscope.

Cell culture

Isolated mouse microvascular endothelial cells and human umbilical vascular endothelial cells (HUVECs) were grown and maintained as instructed by the supplier (Cambrex Bio Science Walkersville, Inc.) or described (46).

Melanoma tumour cells, B16F0 (the spontaneous murine melanoma cell line) and B16F10 (a metastatic clone) were cultured in the Dulbecco's Modified Eagle Medium (DMEM) supplemented with 2 mm l-glutamine, 100 U/ml penicillin, 100 lg/ml streptomycin, and 10% heat-inactivated fetal bovine serum (BSA).

Capillary tube formation angiogenesis assays

Capillary tube formation assays were performed using isolated mouse microvascular endothelial cells as described (6,9).

Purification of AGGF1

Recombinant 6x His-tagged AGGF1 protein was purified from *E. coli* BL21 transformed with pET-28VG5Q-wt using a Ni-NTA agarose column as described (6).

Statistical Analysis

All values are presented as mean ± SEM. Statistical analysis was performed using the two-sample student's *t*-test. A *P* value of less than 0.05 was considered significant.

Supplementary Material

Supplementary Material is available at *HMG* online.

Acknowledgements

We thank Ron Conlon for advice and help with the isolation of mouse embryos and Sun-Ah You and other members of Wang Laboratory for discussions and help.
Conflicts of Interest Statement. None declared.

Funding

This study was supported by NIH/NHLBI grants R01 HL121358 and R01 HL126729, the China National Natural Science Foundation grants (91439129, 31430047, NSFC-J1103514), Hubei Province Natural Science Key Program (2014CFA074), the Chinese National Basic Research Programs (973 Programs 2013CB531101 and 2012CB517801), Hubei Province's Outstanding Medical Academic Leader Program, Specialized Research Fund for the Doctoral Program of Higher Education from the Ministry of Education, and the "Innovative Development of New Drugs" Key Scientific Project (2011ZX09307-001-09).

References

1. Amini, M.R. and Wang, Q.K. (2008) In Epstein C.J., Erickson, R.P., Wynshaw-Boris, A. (eds.), *Inborn Errors of Development*. Oxford University Press, Oxford, New York, pp. 1566–1569.
2. Berry, S.A., Peterson, C., Mize, W., Bloom, K., Zachary, C., Blasco, P. and Hunter, D. (1998) Klippel-Trenaunay syndrome. *Am. J. Med Genet.*, **79**, 319–326.
3. Jacob, A.G., Driscoll, D.J., Shaughnessy, W.J., Stanson, A.W., Clay, R.P. and Gloviczki, P. (1998) Klippel-Trenaunay syndrome: spectrum and management. *Mayo Clin. Proc.*, **73**, 28–36.
4. Timur, A.A., Driscoll, D.J. and Wang, Q. (2005) Biomedicine and diseases: the Klippel-Trenaunay syndrome, vascular anomalies and vascular morphogenesis. *Cell Mol. Life Sci.*, **62**, 1434–1447.

5. Wang, Q.K. (2005) Update on the molecular genetics of vascular anomalies. *Lymphat. Res. Biol.*, **3**, 226–233.
6. Tian, X.L., Kadaba, R., You, S.A., Liu, M., Timur, A.A., Yang, L., Chen, Q., Szafranski, P., Rao, S., Wu, L., *et al.* (2004) Identification of an angiogenic factor that when mutated causes susceptibility to Klippel-Trenaunay syndrome. *Nature*, **427**, 640–645.
7. Chen, D., Li, L., Tu, X., Yin, Z. and Wang, Q. (2013) Functional characterization of Klippel-Trenaunay syndrome gene AGGF1 identifies a novel angiogenic signaling pathway for specification of vein differentiation and angiogenesis during embryogenesis. *Hum. Mol. Genet.*, **22**, 963–976.
8. Hu, Y., Li, L., Seidelmann, S.B., Timur, A.A., Shen, P.H., Driscoll, D.J. and Wang, Q.K. (2008) Identification of association of common AGGF1 variants with susceptibility for Klippel-Trenaunay syndrome using the structure association program. *Ann. Hum. Genet*, **72**, 636–643.
9. Fan, C., Ouyang, P., Timur, A.A., He, P., You, S.A., Hu, Y., Ke, T., Driscoll, D.J., Chen, Q. and Wang, Q.K. (2009) Novel roles of GATA1 in regulation of angiogenic factor AGGF1 and endothelial cell function. *J. Biol. Chem.*, **284**, 23331–23343.
10. Lu, Q., Yao, Y., Yao, Y., Liu, S., Huang, Y., Lu, S., Bai, Y., Zhou, B., Xu, Y., Li, L., *et al.* (2012) Angiogenic factor AGGF1 promotes therapeutic angiogenesis in a mouse limb ischemia model. *PLoS. One*, **7**, e46998.
11. Li, L., Chen, D., Li, J., Wang, X., Wang, N., Xu, C. and Wang, Q.K. (2014) Aggf1 acts at the top of the genetic regulatory hierarchy in specification of hemangioblasts in zebrafish. *Blood*, **123**, 501–508.
12. He, Y., Zhang, H., Yu, L., Gunel, M., Boggon, T.J., Chen, H. and Min, W. (2010) Stabilization of VEGFR2 signaling by cerebral cavernous malformation 3 is critical for vascular development. *Sci. Signal*, **3**, ra26.
13. Lee, S., Chen, T.T., Barber, C.L., Jordan, M.C., Murdock, J., Desai, S., Ferrara, N., Nagy, A., Roos, K.P. and Iruela-Arispe, M.L. (2007) Autocrine VEGF signaling is required for vascular homeostasis. *Cell*, **130**, 691–703.
14. Dejana, E. and Orsenigo, F. (2013) Endothelial adherens junctions at a glance. *J. Cell Sci.*, **126**, 2545–2549.
15. Shiojima, I. and Walsh, K. (2002) Role of Akt signaling in vascular homeostasis and angiogenesis. *Circ. Res.*, **90**, 1243–1250.
16. Carmeliet, P., Ferreira, V., Breier, G., Pollefeyt, S., Kieckens, L., Gertsenstein, M., Fahrig, M., Vandenhoeck, A., Harpal, K., Eberhardt, C., *et al.* (1996) Abnormal blood vessel development and lethality in embryos lacking a single VEGF allele. *Nature*, **380**, 435–439.
17. Ferrara, N., Carver-Moore, K., Chen, H., Dowd, M., Lu, L., O'Shea, K.S., Powell-Braxton, L., Hillan, K.J. and Moore, M.W. (1996) Heterozygous embryonic lethality induced by targeted inactivation of the VEGF gene. *Nature*, **380**, 439–442.
18. Duarte, A., Hirashima, M., Benedito, R., Trindade, A., Diniz, P., Bekman, E., Costa, L., Henrique, D. and Rossant, J. (2004) Dosage-sensitive requirement for mouse Dll4 in artery development. *Genes Dev.*, **18**, 2474–2478.
19. Gale, N.W., Dominguez, M.G., Noguera, I., Pan, L., Hughes, V., Valenzuela, D.M., Murphy, A.J., Adams, N.C., Lin, H.C., Holash, J., *et al.* (2004) Haploinsufficiency of delta-like 4 ligand results in embryonic lethality due to major defects in arterial and vascular development. *Proc. Natl. Acad. Sci. U. S. A*, **101**, 15949–15954.
20. Krebs, L.T., Shutter, J.R., Tanigaki, K., Honjo, T., Stark, K.L. and Gridley, T. (2004) Haploinsufficient lethality and formation of arteriovenous malformations in Notch pathway mutants. *Genes Dev.*, **18**, 2469–2473.
21. Weis, S., Shintani, S., Weber, A., Kirchmair, R., Wood, M., Cravens, A., McSharry, H., Iwakura, A., Yoon, Y.S., Himes, N., *et al.* (2004) Src blockade stabilizes a Flk/cadherin complex, reducing edema and tissue injury following myocardial infarction. *J. Clin. Invest.*, **113**, 885–894.
22. Ito, H. (2006) No-reflow phenomenon and prognosis in patients with acute myocardial infarction. *Nat. Clin. Pract. Cardiovasc. Med.*, **3**, 499–506.
23. John, A.R., Bramhall, S.R. and Eggo, M.C. (2008) Antiangiogenic therapy and surgical practice. *Br. J. Surg.*, **95**, 281–293.
24. Nagy, J.A., Chang, S.H., Shih, S.C., Dvorak, A.M. and Dvorak, H.F. (2010) Heterogeneity of the tumor vasculature. *Semin. Thromb. Hemost.*, **36**, 321–331.
25. Baskerville, P.A., Ackroyd, J.S. and Browse, N.L. (1985) The etiology of the Klippel-Trenaunay syndrome. *Ann. Surg.*, **202**, 624–627.
26. Kurek, K.C., Luks, V.L., Ayturk, U.M., Alomari, A.I., Fishman, S.J., Spencer, S.A., Mulliken, J.B., Bowen, M.E., Yamamoto, G.L., Kozakewich, H.P. and Warman, M.L. (2012) Somatic mosaic activating mutations in PIK3CA cause CLOVES syndrome. *Am. J. Hum. Genet.*, **90**, 1108–1115.
27. Luks, V.L., Kamitaki, N., Vivero, M.P., Uller, W., Rab, R., Bovee, J.V., Rialon, K.L., Guevara, C.J., Alomari, A.I., Greene, A.K., *et al.* (2015) Lymphatic and other vascular malformative/overgrowth disorders are caused by somatic mutations in PIK3CA. *J. Pediatr.*, **166**, 1048–1054.
28. Chen, J., Somanath, P.R., Razorenova, O., Chen, W.S., Hay, N., Bornstein, P. and Byzova, T.V. (2005) Akt1 regulates pathological angiogenesis, vascular maturation and permeability in vivo. *Nat. Med.*, **11**, 1188–1196.
29. Lee, M.Y., Luciano, A.K., Ackah, E., Rodriguez-Vita, J., Bancroft, T.A., Eichmann, A., Simons, M., Kyriakides, T.R., Morales-Ruiz, M. and Sessa, W.C. (2014) Endothelial Akt1 mediates angiogenesis by phosphorylating multiple angiogenic substrates. *Proc. Natl. Acad. Sci. U. S. A*, **111**, 12865–12870.
30. Hers, I., Vincent, E.E. and Tavare, J.M. (2011) Akt signalling in health and disease. *Cell Signal*, **23**, 1515–1527.
31. Dummler, B., Tschopp, O., Hynx, D., Yang, Z.Z., Dirnhofer, S. and Hemmings, B.A. (2006) Life with a single isoform of Akt: mice lacking Akt2 and Akt3 are viable but display impaired glucose homeostasis and growth deficiencies. *Mol. Cell Biol.*, **26**, 8042–8051.
32. Tian, X.L., Yong, S.L., Wan, X., Wu, L., Chung, M.K., Tchou, P.J., Rosenbaum, D.S., Van Wagoner, D.R., Kirsch, G.E. and Wang, Q. (2004) Mechanisms by which SCN5A mutation N(1325)S causes cardiac arrhythmias and sudden death in vivo. *Cardiovasc. Res.*, **61**, 256–267.
33. Zhang, T., Yong, S.L., Tian, X.L. and Wang, Q.K. (2007) Cardiac-specific overexpression of SCN5A gene leads to shorter P wave duration and PR interval in transgenic mice. *Biochem. Biophys. Res. Commun.*, **355**, 444–450.
34. Zhang, X., Chen, S., Yoo, S., Chakrabarti, S., Zhang, T., Ke, T., Oberti, C., Yong, S.L., Fang, F., Li, L., *et al.* (2008) Mutation in nuclear pore component NUP155 leads to atrial fibrillation and early sudden cardiac death. *Cell*, **135**, 1017–1027.
35. LePage, D.F. and Conlon, R.A. (2006) Animal models for disease: knockout, knock-in, and conditional mutant mice. *Methods Mol. Med.*, **129**, 41–67.
36. Zhang, T., Yong, S.L., Drinko, J.K., Popovic, Z.B., Shryock, J.C., Belardinelli, L. and Wang, Q.K. (2011) LQTS mutation N1325S in cardiac sodium channel gene SCN5A causes cardiomyocyte apoptosis, cardiac fibrosis and contractile dysfunction in mice. *Int. J. Cardiol.*, **147**, 239–245.

37. Han, E.D., MacFarlane, R.C., Mulligan, A.N., Scafidi, J. and Davis, A.E., III. (2002) Increased vascular permeability in C1 inhibitor-deficient mice mediated by the bradykinin type 2 receptor. *J. Clin. Invest.*, **109**, 1057–1063.
38. Lin, Z., Natesan, V., Shi, H., Dong, F., Kawanami, D., Mahabeleshwar, G.H., Atkins, G.B., Nayak, L., Cui, Y., Finigan, J.H. and Jain, M.K. (2010) Kruppel-like factor 2 regulates endothelial barrier function. *Arterioscler. Thromb. Vasc. Biol.*, **30**, 1952–1959.
39. Yano, K., Liaw, P.C., Mullington, J.M., Shih, S.C., Okada, H., Bodyak, N., Kang, P.M., Toltl, L., Belikoff, B., Buras, J., *et al.* (2006) Vascular endothelial growth factor is an important determinant of sepsis morbidity and mortality. *J. Exp. Med.*, **203**, 1447–1458.
40. Archacki, S.R., Angheloiu, G., Tian, X.L., Tan, F.L., DiPaola, N., Shen, G.Q., Moravec, C., Ellis, S., Topol, E.J. and Wang, Q. (2003) Identification of new genes differentially expressed in coronary artery disease by expression profiling. *Physiol. Genomics*, **15**, 65–74.
41. Archacki, S.R., Angheloiu, G., Moravec, C.S., Liu, H., Topol, E.J. and Wang, Q.K. (2012) Comparative gene expression analysis between coronary arteries and internal mammary arteries identifies a role for the TES gene in endothelial cell functions relevant to coronary artery disease. *Hum. Mol. Genet.*, **21**, 1364–1373.
42. Wang, F., Xu, C.Q., He, Q., Cai, J.P., Li, X.C., Wang, D., Xiong, X., Liao, Y.H., Zeng, Q.T., Yang, Y.Z., *et al.* (2011) Genome-wide association identifies a susceptibility locus for coronary artery disease in the Chinese Han population. *Nat. Genet.*, **43**, 345–349.
43. You, S.A., Archacki, S.R., Angheloiu, G., Moravec, C.S., Rao, S., Kinter, M., Topol, E.J. and Wang, Q. (2003) Proteomic approach to coronary atherosclerosis shows ferritin light chain as a significant marker: evidence consistent with iron hypothesis in atherosclerosis. *Physiol. Genomics*, **13**, 25–30.
44. Fan, C., Chen, Q. and Wang, Q.K. (2009) Functional Role of Transcriptional Factor TBX5 in Pre-mRNA Splicing and Holt-Oram Syndrome via Association with SC35. *J. Biol. Chem.*, **284**, 25653–25663.
45. Xu, Y., Zhou, M., Wang, J., Zhao, Y., Li, S., Zhou, B., Su, Z., Xu, C., Xia, Y., Qian, H., *et al.* (2014) Role of microRNA-27a in down-regulation of angiogenic factor AGGF1 under hypoxia associated with high-grade bladder urothelial carcinoma. *Biochim. Biophys. Acta*, **1842**, 712–725.
46. Mahabeleshwar, G.H., Somanath, P.R. and Byzova, T.V. (2006) In Wang QK (ed.), *Cardiovascular Disease: Methods and Protocols (Molecular Medicine)*. Humana Press, pp. 197–208.